

On DoF Conservation in MIMO Interference Cancellation based on Signal Strength in the Eigenspace

Yongce Chen, *Member, IEEE*, Shaoran Li, *Student Member, IEEE*,
Chengzhang Li, *Student Member, IEEE*, Huacheng Zeng, *Senior Member, IEEE*,
Brian Jalaian, *Member, IEEE*, Y. Thomas Hou, *Fellow, IEEE*, and Wenjing Lou, *Fellow, IEEE*

Abstract—Degree-of-freedom (DoF)-based models have been proven to be highly successful in modeling and analysis of MIMO systems. Among existing DoF-based models, the number of DoFs used for interference cancellation (IC) is solely based on the number of interfering data streams. However, from both experimental and simulation results, we find that signal strengths of an interference link vary significantly in different directions in the eigenspace. In this paper, we exploit the difference in interference signal strengths in the eigenspace and perform IC with DoFs only on those directions with strong signals. To differentiate interference signal strengths on an interference link, we introduce a novel concept called “effective rank threshold.” Based on this threshold, DoFs are consumed only to cancel strong interferences in the eigenspace while weak interferences are treated as noise in throughput calculation. To better understand the benefits of this approach, we study a fundamental trade-off between network throughput and effective rank threshold for an MU-MIMO network. Our simulation results show that network throughput under optimal rank threshold is significantly higher than that under existing DoF IC models. To ensure the new DoF IC model is feasible at PHY layer, we propose an algorithm to set the weights for all nodes that can offer our desired DoF allocation.

Index Terms—Degree of freedom (DoF), MIMO networks, interference cancellation.

1 INTRODUCTION

DEGREE-of-Freedom (DoF) based models have become widely popular in the research community for modeling, analysis, and optimization of MIMO networks [2–13]. Due to their simple abstraction of MIMO’s capabilities in spatial multiplexing (SM) and interference cancellation (IC) [14–18], a DoF-based model can be used for resource allocation for SM and IC with simple “+/-” arithmetic calculations. By avoiding complex matrix manipulation in resource allocation, DoF-based models are powerful and tractable tools to analyze MIMO’s behavior in a network setting.

Under a DoF-based model, the total number of available DoFs at a node is the same as its number of antennas, and a node can use its DoFs for either SM or IC [2–13]. To understand the limitations of existing DoF model, let’s first re-examine state-of-the-art IC strategies in existing DoF models from the networking research community. Under existing IC schemes, *all* interference at an interference channel are cancelled at either Tx side or Rx side, regardless of interference strength in different directions in the eigenspace

[2–13]. The number of DoFs consumed in IC is solely based on the number of interfering data streams. That is, given the number of transmitting data streams, the number of DoFs required by IC under a highly correlated interference channel would be exactly the same as that under a channel with uniformly distributed singular values, without any discrimination on channel conditions in different directions. However, interference strength varies greatly in different directions in the eigenspace for an interference link, as we shall see in an example (experiment) in Section 2. As a consequence, the existing IC models may not utilize DoF resources efficiently, as they blindly consider the impact of a weak interference signal the same as a strong interference signal.

Related Work In the literature, exploring the difference in signal strengths from different sources/directions has been investigated at PHY layer. Some representative works include channel estimation for low-rank channels [19, 20], estimating the number of sources based on Akaike’s information criterion (AIC) and minimum description length (MDL) techniques [21, 22], and beamforming designs based on interference alignment (IA) technique [23, 24]. However, results of these studies were at the PHY layer and cannot be directly used to address the DoF utilization problems for DoF-based IC in a multi-link MIMO network, which is the focus of this paper.

DoF-based IC models have been actively studied in the Information Theory (IT) and networking communities. In the IT community, DoF characterizations are mainly based on idealized channel models, i.e., either full rank (e.g. [25, 26]) or rank-deficient with zero singular values (e.g.

- An abridged version of this paper appeared in the Proc. IEEE INFOCOM 2019, Paris, France [1].
- Y. Chen is with NVIDIA Corporation, Santa Clara, CA 95054, USA. E-mail: yc.chen@vt.edu
- S. Li, C. Li, Y.T. Hou and W. Lou are with Virginia Tech, Blacksburg, VA 24061 USA. E-mail: {shaoran, lizc17, thou, wjlou}@vt.edu. (Corresponding author: Y.T. Hou)
- H. Zeng is with the Michigan State University, East Lansing, MI 48824 USA. E-mail: hzeng@msu.edu.
- B. Jalaian is with the U.S. Army Research Laboratory, Adelphi, MD 20783 USA. E-mail: brian.a.jalaian.civ@mail.mil.

[27–30]). Such idealized channel rank models do not exactly capture what happens in reality, where singular values for weak interference are not exactly zero. As a result, they cannot closely represent channel behaviors in the real world.

In the networking community, most existing DoF-based models assume that channels are of full rank [2–13]. To measure the footprint of interference (and its impact), the so-called protocol model (or disc model) has been widely used [2–13], where an Rx node within a predetermined interference range is considered interfered and would require DoFs to cancel the interference, while an Rx node outside that range is considered to experience negligible interference (i.e., no IC is needed). The main issue with this model is that, for an Rx node (inside the interference range), it does not differentiate interference strength in different directions in the eigenspace and thus would require DoFs to cancel interference in all directions (for the same Rx node) even though the signal strength in certain directions may be very weak. The weakness of these models is further amplified when the number of antennas at Tx/Rx nodes becomes large and channels exhibit high correlation. As a result, these models cannot exploit the full potential of MIMO networks. In contrast, instead of using a disc (or interference range), this paper proposes to differentiate interference strength by examining singular values in the eigenspace regardless of the location of the Rx node. Strong interferences (corresponding to large singular values) are cancelled by DoFs while weak interferences (corresponding to small singular values) are treated as noise in throughput calculation. This approach provides efficient DoF utilization that can offer higher throughput.

Scope and Contributions In this paper, we aim to improve DoF utilization for DoF-based IC studies for the networking community. We propose to exploit the differences in interference signal strength among different directions by examining singular values in the eigenspace and propose to expend DoFs only to cancel strong interference. In other words, we want to conserve precious DoFs from cancelling the weaker ones. Specifically, we introduce the concept called “effective rank threshold.” If the singular value (i.e., the interference strength at the corresponding direction in the eigenspace) is greater than the threshold, then such interference will be cancelled with DoFs. But if the singular value is smaller than effective rank threshold, it will be treated as noise before IC. Although there might be throughput loss due to uncancelled weak interference, precious DoFs can be saved to support more data streams which in return improves network throughput. The main contributions of this paper are summarized as the following:

- This is the first paper on DoF-based IC strategies in networking research that exploits interference signal strengths in the eigenspace. Existing DoF models cancel interference with precious DoFs on all directions in the eigenspace. Instead, we propose to perform IC with DoFs only on those directions with strong signals in the eigenspace.
- We introduced the concept of effective rank threshold to differentiate strong and weak interference in different directions in the eigenspace on an interference link. Based on this effective rank threshold, IC

will only be performed for strong interference corresponding to large singular values in the eigenspace, while weak interference will be treated as noise in throughput calculation.

- We investigate the fundamental trade-off between throughput and effective rank threshold, using a general MU-MIMO network. Through simulation results, we show that there exists an optimal trade-off between throughput and effective rank threshold. We show that the network throughput under optimal effective rank threshold setting is considerably higher than that under existing DoF models.
- To ensure our new IC model is feasible at the PHY layer, we propose an algorithm to determine weights for all Tx and Rx nodes that can offer our desired DoF allocation. Through an iterative process, our algorithm can successfully find the beamforming weights for all Tx and Rx nodes such that the strong interferences beyond the effective rank threshold can be suppressed close to zero, thus ensuring the feasibility of our new IC model.

The remainder of this paper is organized as follows. In Section 2, we use a motivating example to illustrate our new IC idea. Section 3 shows how to determine the effective channel rank of a link. In Section 4, we present the DoF IC model based on effective channel rank. Section 5 analyzes the trade-off among total network throughput, DoFs for SM, and effective channel rank. In Section 6, we develop an algorithm that can find Tx and Rx weights at each node to ensure feasibility at PHY layer. Section 7 concludes this paper.

2 A MOTIVATING EXAMPLE

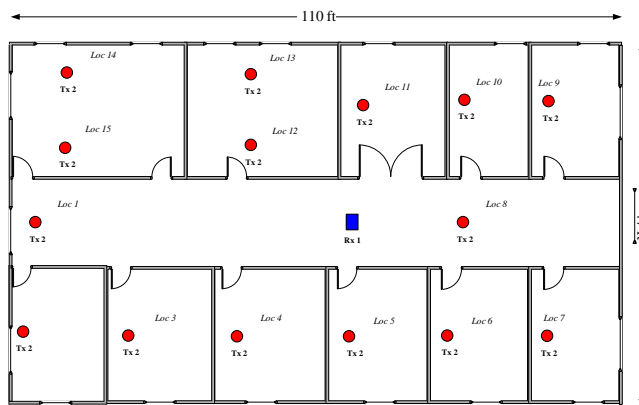
In this section, we first use an experiment to examine the disparity in singular values of a link. Then we use a motivating example to illustrate our main idea.

An Experiment We have conducted experiments to examine channel conditions in an indoor environment. In this experiment, we build two nodes to form an 8×8 MIMO channel. Each node is built with 8 USRP N210 devices [31], a OctoClock-G CDA-2990 device [32], a 10 GbE-switch, a desktop computer, and GNU radio software package [33]. The 8 USRP devices are connected to the 10 GbE-switch via CAT5E Ethernet cables and synchronized using the OctoClock-G CDA-2990 device (providing external 1 PPS and 10 MHz reference clock), as shown in Fig. 1(a). We install GNU Radio (in Ubuntu) on the desktop computer to control the USRP devices. Such a MIMO node can achieve 25 MHz of instantaneous bandwidth (52 sub-carriers) in 2.1 GHz band for wireless signal transmission and reception. We perform a set of experiments under LOS/NLOS with linear or rectangular arrays in an indoor environment to measure the MIMO channel matrices. The floor plan is shown in Fig. 1(b), where LOS and NLOS channels are measured when the Tx node is located at locations 8 and 13, respectively.

Then we perform singular value decomposition (SVD) of measured 8×8 MIMO channel matrices. Fig. 2 presents the singular values in each direction under different settings. As shown in Fig. 2, deficient channel rank (lower than the



(a) A portable 8-antenna wireless testbed.



(b) The floor plan of channel measurement scenario.

Fig. 1: An experiment to measure channel matrices.

number of Tx/Rx antennas) can be seen throughout our experiments, i.e., zero or near-zero for the least singular value. More important, in many cases, we observe that the remaining singular values vary greatly. This means signals in some directions are much stronger than the others on the same link. This phenomenon is mainly due to the lack of rich multipath propagation and spatial separations, leading to correlations among the spatial channels within the MIMO link [34, 35]. As a result, the transmit power from a node is generally not uniformly distributed in all directions of the channel's eigenspace. ■

Based on our observation from the experiment, we ask the following question: Can we exploit such disparity in singular values (interference signal strength) to conserve DoF in IC? Now we use the following example to illustrate our main idea.

Considering a simple two-cell MIMO network shown in Fig. 3. There are two APs (AP1 and AP2) and two users (u_1 and u_2). Suppose each node (AP or user) is equipped with 12 antennas. AP1 transmits z_{11} data streams to user u_1 (marked with solid arrow lines) which interfere with user u_2 (marked with dashed arrow lines). Likewise, AP2 transmits concurrently z_{22} data streams to user u_2 . For the time being,

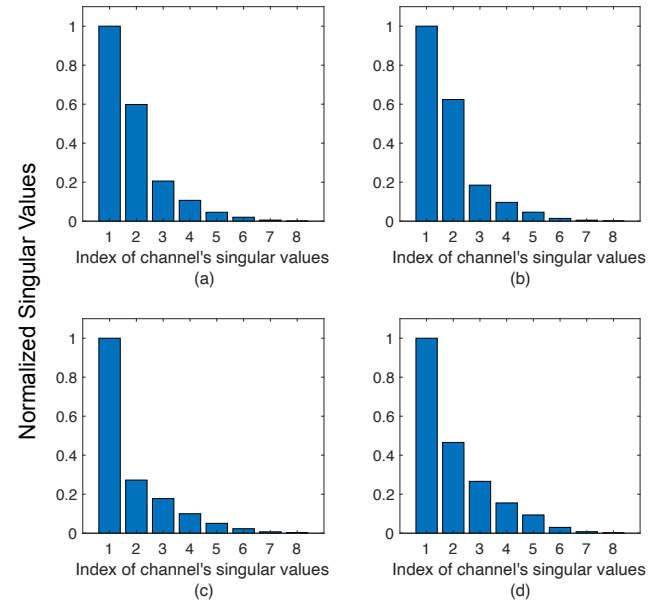


Fig. 2: SVD of an 8×8 MIMO channel in our experiment. Carrier frequency is 2.1 GHz. Antenna spacing is 5 cm. (a) LOS channel with linear array. (b) NLOS channel with linear array. (c) LOS channel with rectangular array. (d) NLOS channel with rectangular array.

let's neglect the interference from AP2 to user u_1 .¹

Consider the interference channel \mathbf{H}_{12} in Fig. 3. We use the Kronecker channel model to characterize the channel correlations [35]. We can write \mathbf{H}_{12} as $\mathbf{H}_{12} = \mathbf{R}_{tx}^{1/2} \mathbf{H}_w \mathbf{R}_{rx}^{1/2}$, where \mathbf{H}_w is an 12×12 random matrix with zero-mean i.i.d. complex Gaussian entries, $\mathbf{R}_{tx}^{1/2}$ ($\mathbf{R}_{rx}^{1/2}$) is the 12×12 square root matrix of the transmit (receiver) antenna correlation matrix. The (i, j) -th element in the correlation matrix \mathbf{R}_{tx} and \mathbf{R}_{rx} is calculated as $\rho_{tx}^{|i-j|}$ and $\rho_{rx}^{|i-j|}$, where $\rho_{tx} \in [0, 1]$ and $\rho_{rx} \in [0, 1]$ represent the level of correlation between any two adjacent antennas (in a linear antenna array) at the respective Tx and Rx nodes [36, 37].

For different values of ρ_{tx} and ρ_{rx} , we can simulate the expectations of singular values σ of $\mathbf{H}_{12}^H \mathbf{H}_{12}$, which we show in Fig. 4. It is easy to see that for any given value of ρ_{tx} and ρ_{rx} , the expectations of singular values vary significantly, which is consistent with our experimental result for the 8×8 MIMO channel case in Fig. 2. Here, a high singular value indicates that a large portion of AP1's power is projected into the direction of the corresponding singular vector. Likewise, a close-to-zero singular value indicates a close-to-zero portion of AP1's power is projected into the direction of the corresponding singular vector. When the values of ρ_{tx} and ρ_{rx} increases (i.e., with increased channel correlation), more and more expectations of singular values diminish toward zero.²

Figure 4 suggests that the interference strength varies significantly in different directions in its eigenspace. Under traditional IC scheme (see, e.g., [2–11]), all interference from

¹ Such weak interference will be considered in throughput calculation (see Section 5).

² Apart from correlation, singular values can also be zero due to the presence of "key-hole" effect [38, 39].

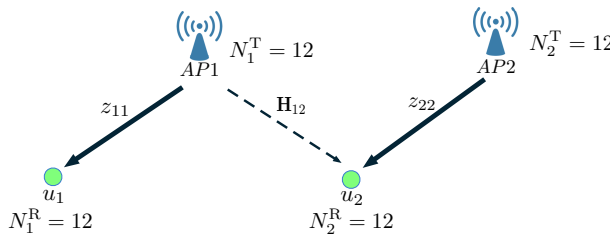


Fig. 3: A motivating example with two APs and two users.

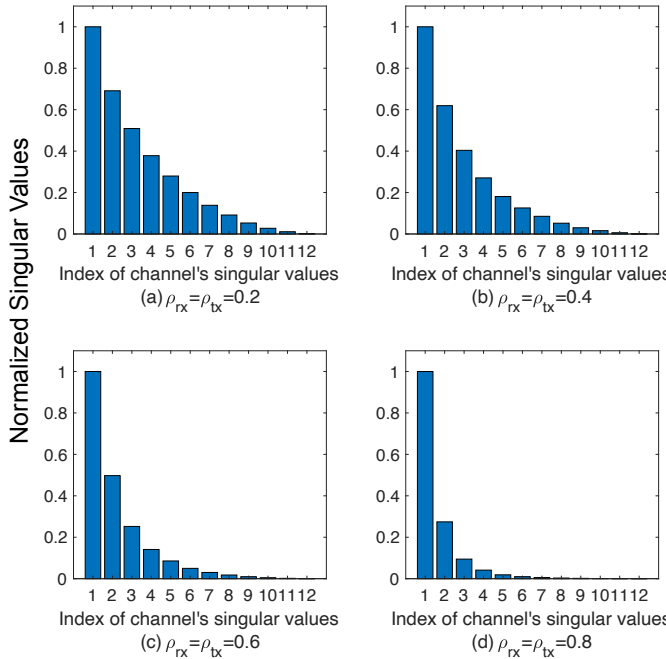


Fig. 4: Simulation results of expectations of singular values $E[\sigma]$ under different levels of correlation (ρ_{tx} and ρ_{rx}).

AP1 to u_2 shall be cancelled by either AP1 (Tx side, using z_{22} DoFs) or u_2 (Rx side, using z_{11} DoFs). This approach does not differentiate strong and weak interferences in different directions and thus blindly cancels them all with precious DoFs.

To explore this potential opportunity, we propose to exploit the difference of interference power strength in each direction and only cancel the strong interference with DoFs while treating the weak ones just as noise. In other words, by exploiting the disparity in interference signal strengths in the eigenspace, we could conserve precious DoFs from cancelling the weaker ones.

Specifically, as shown in Fig. 4 ((c) and (d) in particular), the vast majority interference power only appears in the directions corresponding to the high singular values of \mathbf{H}_{12} , which can be properly cancelled by using a small number of DoFs. But the remaining weak (small) interference power in these figures is better treated as noise, rather than to be cancelled with precious DoFs. Although there may be some throughput loss due to un-cancelled weak interference, the DoFs savings could be used to transport more data streams (SM). By judiciously exploiting the threshold used to differentiate strong and weak interference, one could achieve a better design objective (e.g., more data streams and/or

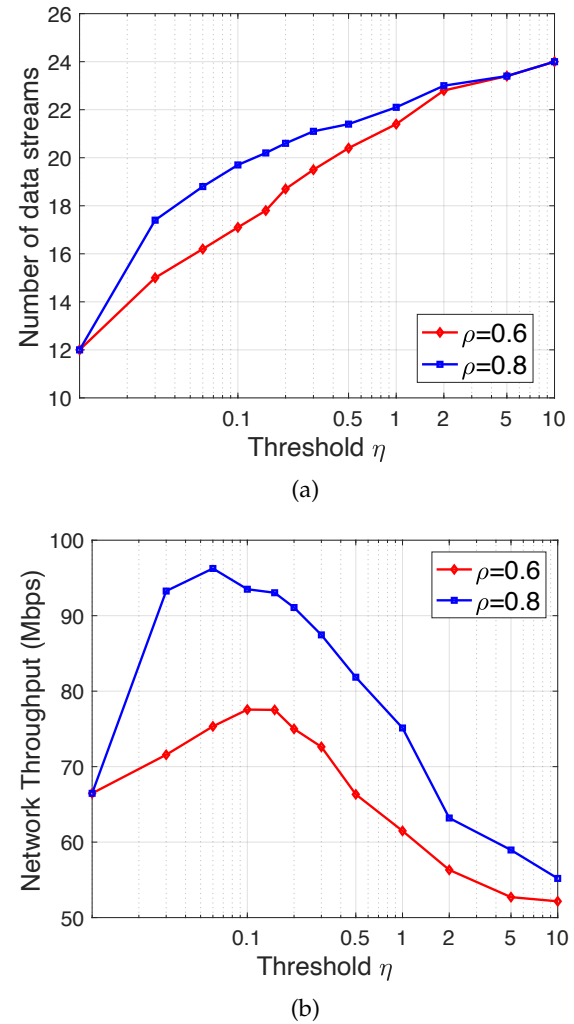


Fig. 5: Total DoFs for SM and throughput performance as a function of threshold setting (used to differentiate strong and weak interferences). (a) Total number of data streams in the network. (b) Network throughput.

higher throughput) than blindly cancelling all interferences (weak or strong) with DoFs, as in existing approaches [2–11].

To show the potential benefits, suppose we set $z_{11} = 12$ in the example in Fig. 3. Following traditional IC approach (i.e., no differentiation between strong and weak interferences), AP2 cannot send any data stream to user u_2 as there is no DoF left at user u_2 to cancel interference from AP1. On the other hand, if u_2 treats the interference coming from AP1 in the direction corresponding to the least singular value of \mathbf{H}_{12} as weak interference and does not use a DoF to cancel it, then it only needs to use 11 DoFs for IC from AP1 to u_2 and use the remaining one to support one data stream transmission from AP2 to u_2 . Following the same token, as more interferences from AP1 (corresponding to the least singular values) are treated as weak interferences and thus not to be cancelled with DoFs, more DoFs could be saved and be used to support SM from AP2 to u_2 .

As shown in Fig. 5(a), by increasing interference threshold η (more on this notation in Section 3) to differentiate strong and weak interferences, more DoFs can be conserved

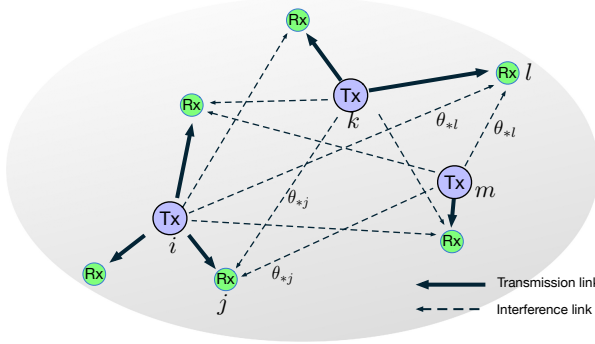


Fig. 6: A general MU-MIMO network with multiple Tx nodes and Rx nodes.

from cancelling a fewer number of weak interferences at u_2 and more data streams (SM) can be sent from AP2 to u_2 . Fig. 5(b) shows the total network throughput on all data streams (from AP1 to u_1 and AP2 to u_2) as a function of interference threshold η . Clearly, there is a trade-off among total network throughput, DoFs for SM, and effective channel rank. In particular, there is an optimal knee point that offers the best trade-off between total throughput and effective channel rank (determined by interference threshold η).

3 DETERMINE EFFECTIVE CHANNEL RANK OF A LINK

In this section, we present the system model and introduce the concept of “effective channel rank.” Consider a general MU-MIMO network (see Fig. 6) with a set \mathcal{K}^T of Tx nodes and a set \mathcal{K}^R of Rx nodes, respectively. Each Tx node $i \in \mathcal{K}^T$ and Rx node $j \in \mathcal{K}^R$ are equipped with N_i^T and N_j^R antennas, respectively. Under MU-MIMO, a Tx node is able to transmit to multiple Rx nodes concurrently while each Rx node can receive from at most one Tx node. For a Tx node $i \in \mathcal{K}^T$, denote \mathcal{K}_i^R as the set of its Rx nodes. For an Rx node $j \in \mathcal{K}^R$, denote $s(j)$ as its source Tx node. Table 1 lists key notations in this paper.

3.1 Effective Rank of A Single Interference Link

We first differentiate strong and weak interferences on a single interference link and use this differentiation to determine its effective rank. For a single interference link $k \rightarrow j$, instead of dealing directly with the fast fading channel matrix $\mathbf{H}_{kj} \in \mathbb{C}^{N_k^T \times N_j^R}$, we take into consideration of transmit power and path loss fading. Denote P_k as the transmit power at Tx node k and L_{kj} as the path loss from Tx node k to Rx node j . Define \mathbf{Y}_{kj} (an $N_j^R \times N_j^R$ symmetric matrix) as the perceived channel covariance matrix at Rx node j for the link $k \rightarrow j$:

$$\mathbf{Y}_{kj} = \frac{P_k L_{kj}}{N_k^T} \mathbf{H}_{kj}^H \mathbf{H}_{kj}, \quad (1)$$

where \mathbf{X}^H is the conjugate transpose of \mathbf{X} . In matrix \mathbf{Y}_{kj} , each entry represents the received interference power on the corresponding channel on interference link $k \rightarrow j$. We will use \mathbf{Y}_{kj} to determine the effective rank of interference link $k \rightarrow j$.

TABLE 1: Notation

Symbol	Definition
d_{ij}^R	Number of DoFs consumed by Rx node j to cancel interference from Tx node i to Rx node j
d_{ij}^T	Number of DoFs consumed by Tx node i to cancel interference from Tx node i to Rx node j
\mathbf{H}_{ij}	Channel matrix from Tx node i to Rx node j
\mathcal{K}^T	Set of Tx nodes
\mathcal{K}^R	Set of Rx nodes
\mathcal{K}_i^R	Set of Rx nodes for Tx node i
L_{ij}	Pathloss from Tx node i to Rx node j
N_j^R	Number of antennas at Rx node j
N_i^T	Number of antennas at Tx node i
P_i	Transmission power at Tx node i
r_{ij}	Effective rank of \mathbf{H}_{ij}
$s(j)$	Rx node j 's serving Tx node
\mathbf{U}_i	Weight matrix at Tx node i
\mathbf{V}_j	Weight matrix at Rx node j
z_{i*}	Total number of outgoing data streams at Tx node i
z_{*j}	Total number of incoming data streams at Rx node j
z_{ij}	Number of data streams from Tx node i to Rx node j
η	Normalized effective rank threshold
$\mathbf{X}^{[s,f]}$	The f -th column of matrix \mathbf{X}
\mathbf{X}^H	Conjugate transpose of matrix \mathbf{X}

To differentiate strong and weak interferences, we employ the so-called *best rank- r approximation* of a matrix [40]. Under this approximation, \mathbf{Y}_{kj} is decomposed through an SVD process and we retain only the first r largest singular values and their corresponding singular vectors and use them as an approximation.

Fact 1 For a matrix $\mathbf{A} \in \mathbb{C}^{m \times n}$ ($m \geq n$), denote $\tilde{\mathbf{A}}$ as a rank- r matrix approximation of \mathbf{A} with $r \in \{1, 2, \dots, n\}$. The optimal solution to minimum approximation error

$$\min_{\tilde{\mathbf{A}} \in \mathbb{C}^{m \times n}} \|\mathbf{A} - \tilde{\mathbf{A}}\|_F, \quad \text{s.t. } \text{rank}(\tilde{\mathbf{A}}) = r \quad (2)$$

where $\|\cdot\|_F$ denotes Frobenius norm, is

$$\tilde{\mathbf{A}} = \sum_{i=1}^r \sigma_i \mathbf{u}_i \mathbf{v}_i^H,$$

where σ_i , \mathbf{u}_i , and \mathbf{v}_i are singular value, left and right singular vectors respectively from the SVD of \mathbf{A} , i.e., $\mathbf{A} = \sum_{i=1}^n \sigma_i \mathbf{u}_i \mathbf{v}_i^H$ and $\sigma_1 \geq \sigma_2 \geq \dots \geq \sigma_n$. The minimum approximation error (i.e., optimal objective value for (2)) is $\sqrt{\sum_{i=r+1}^n \sigma_i^2}$.

The SVD process in Fact 1 clearly shows the relative strength of interferences in different directions. The larger the singular value is, the stronger the interference in that direction. Based on the desired level of approximation error, we can approximate a rank- n matrix \mathbf{A} by a rank- r matrix $\tilde{\mathbf{A}}$ with the r -strongest singular values of \mathbf{A} through (1).

To apply best rank- r approximation on a single interference link \mathbf{Y}_{kj} , define θ as a threshold for singular values and denote r_{kj} as the effective channel rank of \mathbf{H}_{kj} . Then r_{kj} is given by

$$r_{kj} = \sum_{l=1}^{N_j^R} \mathbb{1}\{\sigma_l(\mathbf{Y}_{kj}) \geq \theta\}, \quad (3)$$

where $\sigma_l(\mathbf{Y}_{kj})$ is the l -th singular value based on SVD of \mathbf{Y}_{kj} , and $\mathbb{1}\{\text{event}\}$ is an indicator function, which is 1 if event is true and 0 otherwise.

3.2 Interference Threshold at an Rx Node

The setting of effective channel rank can be determined by the threshold θ in (3) for eigenvalues of the interference perceived at Rx nodes. However, in a network with a set of Tx and Rx nodes and multiple interference links, one cannot simply apply the same absolute threshold value for all Rx nodes. This is because throughput is measured in a signal-to-interference ratio sense while the received power from intended transmitter differs at Rx nodes depending on their locations. An Rx node with higher signal power (from its intended transmitter) could tolerate a stronger interference. As a consequence, the interference threshold (used to distinguish strong/weak signals) differs at each Rx node. As an example, consider Rx nodes j and l in Fig. 6. Rx node j is closer to its (intended) Tx node i than Rx node l to its (intended) Tx node k . For the same transmit power at i and k , Rx node j will receive a higher signal power (from its intended transmitter) and could thus tolerate a stronger interference. Then, for the interference links at Rx node j ($k \rightarrow j$ and $m \rightarrow j$), the threshold used to differentiate strong and weak interference should be larger than that used to differentiate stronger and weak interference on interference links ($i \rightarrow l$ and $m \rightarrow l$) for Rx node l . Based on the above discussions, for an Rx node j , denote θ_{*j} as the threshold for singular values on its interference link. Then we should have $\theta_{*j} > \theta_{*l}$.

Although we let each Rx node have its individual threshold θ_{*j} , it is not easy to present results and demonstrate our idea if all the θ_{*j} 's are optimized independently. To address this issue, we introduce a common scaling factor η , which is defined by the rank threshold θ_{*j} normalized by Rx node j 's received intended signal power, i.e.,

$$\theta_{*j} = \eta \frac{P_{s(j)} L_{s(j)j}}{N_{s(j)}^T}.$$

Therefore, instead of optimizing the settings of θ_{*j} for each individual Rx node j , we simply optimize the common factor η across all received nodes. As we will show in our simulation results, this is sufficient to demonstrate the main idea of this paper. It is possible to optimize each threshold θ_{*j} independently with higher complexity, which we leave for future work.

Based on this definition of common scaling factor η , the effective rank r_{kj} of \mathbf{H}_{kj} can be determined by the number of \mathbf{Y}_{kj} 's singular values that are greater than or equal to the threshold $\eta \frac{P_{s(j)} L_{s(j)j}}{N_{s(j)}^T}$. That is,

$$r_{kj} = \sum_{l=1}^{N_j} \mathbb{1} \left\{ \sigma_l(\mathbf{Y}_{kj}) \geq \eta \frac{P_{s(j)} L_{s(j)j}}{N_{s(j)}^T} \right\}, \quad k \in \mathcal{K}^T, j \in \mathcal{K}^R, j \notin \mathcal{K}_i^R, \quad (4)$$

where \mathbf{Y}_{kj} is the channel covariance matrix perceived at Rx node j for the link $k \rightarrow j$, as defined in Eq. (1).

Note that any negligible interference for IC will be treated as noise in the throughput calculation (see Section 5).

3.3 Effective Rank of An SM Link

For SM from node i to node j (intended transmission), the effective channel rank of \mathbf{H}_{ij} can be determined by

$$r_{ij} = \sum_{l=1}^{N_j^R} \mathbb{1} \left\{ \sigma_l(\mathbf{H}_{ij}^H \mathbf{H}_{ij}) \geq \theta_{SM} \right\}, \quad i \in \mathcal{K}^T, j \in \mathcal{K}_i^R,$$

where θ_{SM} is the rank threshold for singular values on SM link $i \rightarrow j$. Note that the DoF savings by exploiting strong and weak interference can be made available for SM (more independent data streams) or diversity, both of which have the potential to increase the throughput. To focus on using DoFs for IC at interference links, we do not explore SM-diversity trade-off in this paper. Therefore, we will try to transmit more data streams as long as we have DoFs available for SM and assume θ_{SM} is a given constant throughout the paper.

3.4 Channel Model

We consider the following channel model unless otherwise stated. Considering a high SNR setting, we assume each Tx node has a fixed (constant) transmit power $P_i = 36$ dBm. The background noise power is set to -169 dBm/Hz and the channel bandwidth is 10 MHz. The path loss fading L_{ij} is given by $140.7 + 36.7 \log_{10}(D_{i,j})$ (in dB) (as suggested by 3GPP for small cells [41]), where $D_{i,j}$ is the distance between Tx node i and Rx node j (in km). For fast fading channel \mathbf{H}_{ij} , it is modeled by Kronecker channel model, i.e., $\mathbf{H}_{ij} = \mathbf{R}_{tx}^{1/2} \mathbf{H}_w \mathbf{R}_{rx}^{1/2}$, where $\mathbf{R}_{rx}^{1/2}$ is an $N_j^R \times N_j^R$ matrix with each entry containing square root of the receive antenna correlation while $\mathbf{R}_{tx}^{1/2}$ is an $N_i^T \times N_i^T$ matrix with each entry containing square root of the transmit antenna correlation. \mathbf{H}_w is an $N_i^T \times N_j^R$ random matrix with its entries containing zero-mean i.i.d. complex Gaussian random numbers. The (k,l) -th element of the correlation matrix \mathbf{R}_{rx} and \mathbf{R}_{tx} is taken here as $\rho^{|k-l|}$ and $\rho \in [0, 1]$ is the correlation level.

We assume a centralized network and all channel state information (CSI) is sent to a central controller. How to estimate and feedback CSI in a MIMO network has been widely investigated in the literature. For a static network, although a wireless channel is time-variant, it changes rather slowly and the channel has a long coherent time. This allows us to obtain relatively accurate CSI with infrequent updates. In such an environment, the overhead in CSI acquisition tends to be acceptable and has been investigated in literature [42–48]. These studies showed practical designs to obtain CSI at the transmitter side in a stationary network with acceptable overhead.

4 IC BASED ON EFFECTIVE CHANNEL RANK

In the last section, we showed how to differentiate strong and weak interference at an Rx node by setting a threshold for singular value and use this threshold to determine effective channel rank. In this section, we show how to perform IC (for strong interference only) in an MU-MIMO network based on this effective channel rank.

Note that DoF allocation for IC cannot be done arbitrarily and must follow certain rules to be feasible. By “feasible”, we mean that all the strong interference can be cancelled at

the PHY layer. Section 6 will present details on PHY layer feasibility for our DoF allocation.

If DoF allocation for IC and SM is feasible at the PHY layer, then multiple data streams can be transmitted concurrently while all strong interference under best rank- r channels is cancelled. The remaining (un-cancelled) weak interference will be treated as noise and included in the throughput calculation in Section 5.

We employ the DoF-based IC model in [49] to perform DoF allocation. In [49], the rank of a channel is assumed to be given *a priori*. But in this paper, the rank of a channel is a function of effective rank threshold.

4.1 Modeling of DoF Constraints

DoF Constraints for SM For an intended transmission from Tx node i to Rx node j , denote the number of data streams on this link as z_{ij} . Denote $x_i(t)$ as a binary variable to indicate whether Tx node i is active or not at time t , i.e., $x_i(t) = 1$ if Tx node i is transmitting at time t and 0 otherwise. Likewise, denote $y_j(t)$ as a binary variable to indicate whether Rx node j is active or not at time t , i.e., $y_j(t) = 1$ if Rx node j is receiving at time t and 0 otherwise.

If Tx node i is transmitting, then the total number of data streams transmitted to different receivers (under MU-MIMO) cannot exceed the total number of antennas at node i (i.e., N_i^T). We have

$$x_i(t) \leq \sum_{j \in \mathcal{K}_i^R} z_{ij}(t) \leq N_i^T x_i(t), \quad i \in \mathcal{K}^T. \quad (5)$$

Similarly, if Rx node j is active at time t , then the total number of DoFs used for reception (from only one transmitter under MU-MIMO) cannot exceed the number of antennas at node j (i.e., N_j^R). We have

$$y_j(t) \leq z_{ij}(t) \leq N_j^R y_j(t), \quad i \in \mathcal{K}^T, j \in \mathcal{K}_i^R. \quad (6)$$

Taking into consideration of the effective rank of the SM link $i \rightarrow j$, the number of data streams that can be sent on this SM link cannot exceed the link's effective rank (see Section 3). We have

$$z_{ij}(t) \leq r_{ij}(t), \quad i \in \mathcal{K}^T, j \in \mathcal{K}_i^R. \quad (7)$$

For Rx node l that is not Tx node i 's intended receiver, i.e., $l \notin \mathcal{K}_i^R$, the transmission at Tx node i is considered interference (instead of SM) and there is zero data streams over this link. We have

$$z_{il}(t) = 0, \quad k \in \mathcal{K}^T, l \in \mathcal{K}^R, l \notin \mathcal{K}_i^R. \quad (8)$$

DoF Constraints for IC For interference from Tx node k to Rx node j , denote $d_{kj}^T(t)$ as the number of consumed DoFs at Tx node k and $d_{kj}^R(t)$ as the number of consumed DoFs at Rx node j that are needed to cancel this interference. Based on [49], a collaborative DoF consumption at both interfering Tx node k and Rx node j is the most efficient approach for IC when the rank of the interference channel is not full, as in our case. Denote $\mathbf{1}_{kj}^T$ and $\mathbf{1}_{kj}^R$ as two binary variables to indicate whether Tx node i (or Rx node j) consumes any DoFs for IC from k to j . That is, $\mathbf{1}_{kj}^T = 1$ if Tx node k consumes DoFs for IC from k to j , $\mathbf{1}_{kj}^T = 0$ otherwise;

$\mathbf{1}_{kj}^R = 1$ if Rx node j consumes DoFs for IC from k to j , $\mathbf{1}_{kj}^R = 0$ otherwise.

If $x_k(t) = 1$ and $y_j(t) = 1$, then

$$\begin{aligned} & d_{kj}^T(t) \mathbf{1}_{kj}^T(t) + d_{kj}^R(t) \mathbf{1}_{kj}^R(t) = \\ & \min \left\{ \mathbf{1}_{kj}^R(t) \sum_{l \in \mathcal{K}_k^R} z_{kl}(t) + \mathbf{1}_{kj}^T(t) \sum_{i \in \mathcal{K}^T} z_{ij}(t), r_{kj}(t) \right\}, \end{aligned} \quad (9a)$$

$$(\mathbf{1}_{kj}^T(t), \mathbf{1}_{kj}^R(t)) \neq (0, 0), \quad k \in \mathcal{K}^T, j \in \mathcal{K}^R \quad (9b)$$

That is, the interference from k to j can be cancelled by consuming DoFs on Tx node k only (when $(\mathbf{1}_{kj}^T(t), \mathbf{1}_{kj}^R(t)) = (1, 0)$), Rx node only (when $(\mathbf{1}_{kj}^T(t), \mathbf{1}_{kj}^R(t)) = (0, 1)$), or both Tx and Rx nodes (when $(\mathbf{1}_{kj}^T(t), \mathbf{1}_{kj}^R(t)) = (1, 1)$). Constraint (9) can be reformulated as mixed integer linear (MIL) constraints, which is omitted here to conserve space.

DoF Constraints at A Node A node can use its DoFs for SM and/or IC, as long as the total number of consumed DoFs does not exceed the total available DoFs at the node. We consider DoF constraints at Tx and Rx nodes separately. If node i is an active Tx node, we have

$$\text{if } x_i(t) = 1, \text{ then } \sum_{j \in \mathcal{K}_i^R} z_{ij}(t) + \sum_{l \in \mathcal{K}^R} d_{il}^T(t) \mathbf{1}_{il}^T(t) \leq N_i^T, \quad i \in \mathcal{K}^T. \quad (10)$$

If node j is an active Rx node, we have

$$\text{if } y_j(t) = 1, \text{ then } \sum_{i \in \mathcal{K}^T} z_{ij}(t) + \sum_{k \in \mathcal{K}^R} d_{kj}^R(t) \mathbf{1}_{kj}^R(t) \leq N_j^R, \quad j \in \mathcal{K}^R. \quad (11)$$

For constraint (10), it can be reformulated by incorporating binary variable $x_i(t)$ into the expression as follows:

$$\sum_{j \in \mathcal{K}_i^R} z_{ij}(t) + \sum_{l \in \mathcal{K}^R} d_{il}^T(t) \mathbf{1}_{il}^T(t) \leq N_i^T x_i(t) + (1 - x_i(t))B, \quad i \in \mathcal{K}^T, \quad (12)$$

where B is a large constant, which can be set as $B = \sum_{i \in \mathcal{K}^T} N_i^T + \sum_{j \in \mathcal{K}^R} N_j^R$ to ensure that B is an upper bound of $\sum_{l \in \mathcal{K}^R} d_{il}^T(t)$.

Similarly, constraint (11) can be reformulated as follows:

$$\sum_{i \in \mathcal{K}^T} z_{ij}(t) + \sum_{k \in \mathcal{K}^R} d_{kj}^R(t) \mathbf{1}_{kj}^R(t) \leq N_j^R y_j(t) + (1 - y_j(t))B, \quad j \in \mathcal{K}^R. \quad (13)$$

Constraints (12) and (13) can be reformulated as mixed integer linear constraints, which are omitted here to conserve space.

4.2 An Example

As an example to illustrate the relationship between total achievable data streams (SM) in the network and η (the common scaling factor to differentiate strong and weak interference and effective channel rank), consider the simple MU-MIMO network in Fig. 7. Suppose our objective is to maximize the sum of log of all data streams (SM) in the

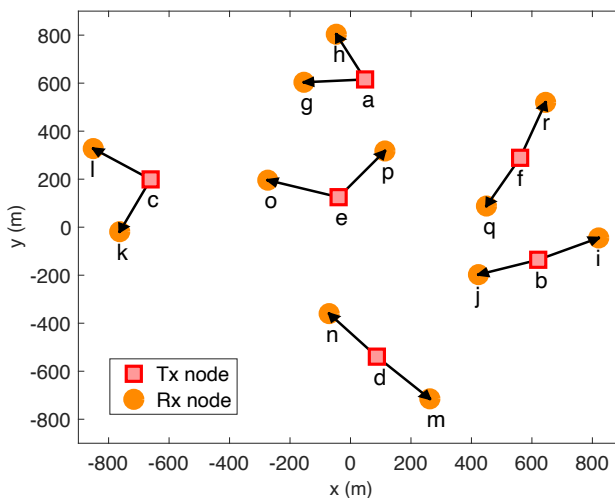


Fig. 7: An instance of MU-MIMO network topology.

network with the consideration of fairness [50]. Then we have the following optimization problem:

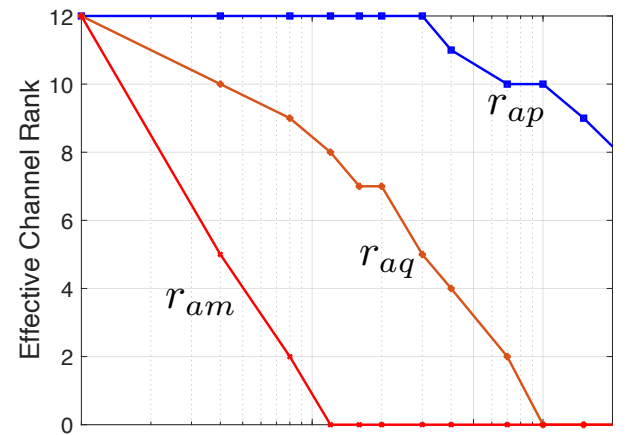
$$\begin{aligned} \max & \sum_{i \in \mathcal{K}^T} \sum_{j \in \mathcal{K}^R} \log(z_{ij}) \\ \text{s.t.} & \text{SM constraints: (5) – (8);} \\ & \text{IC constraints: (9);} \\ & \text{Node's DoF constraints: (12), (13),} \end{aligned}$$

where z_{ij} , d_{kj}^T , d_{kj}^R , $\mathbf{1}_{kj}^T$ and $\mathbf{1}_{kj}^R$ are variables while all other symbols are constants.

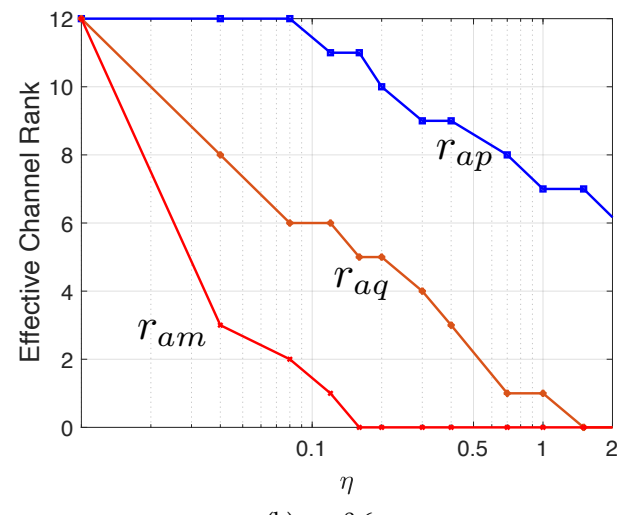
As discussed earlier, the constraints in the above formulation can be reformulated into mixed integer linear constraints. However, the objective function (sum of log) remains non-linear. Fortunately, the sum of log objective can be reformulated (along with the MIL constraints) as a second order conic program (SOCP) [51]. Off-the-shelf optimization tools, such as Gurobi [52], can solve this SOCP (with integer variables) optimally.

Some numerical results follow. Suppose the six Tx nodes in Fig. 7 are uniformly generated in a circle within a radius of 700 m with a minimum of 200 m distance between every two Tx nodes. For each Tx node, there are two Rx nodes uniformly generated with a radius of 250 m of the Tx node. Each Tx and Rx nodes are equipped with 16 and 12 antennas, respectively. We follow the channel model described in Section 3.4, and the correlation level ρ is chosen from {0.2, 0.4, 0.6}.

Fig. 8 shows the effective ranks on three representative links ($a \rightarrow p$, $a \rightarrow q$ and $a \rightarrow m$) as a function of rank threshold scaling factor η (in log scale). We draw η in log scale since singular value distribution is more like a log-shape other than a linear shape (see Fig. 4). As expected, all effective channel ranks are decreasing steadily. For $\rho = 0.2$ shown in Fig. 8(a), note that r_{ap} remains full rank until η becomes greater than 0.4 while r_{aq} and r_{am} starts to decrease when η starts to increase from 0. This is because Rx node p is close to the interfering Tx node a than q and m and thus experience much stronger interference from Tx node a than q and m . On the other hand, r_{am} drops very fast because Rx node m is further away from Tx node a than p and q . When



(a) $\rho = 0.2$



(b) $\rho = 0.6$

Fig. 8: Effective ranks on interference links versus rank threshold scaling factor η .

η is greater than 0.12, $r_{am} = 0$ and Rx node m is considered out of interference range of Tx node a . For $\rho = 0.6$ shown in Fig. 8(b), effective ranks have a similar trend but drop faster than those when $\rho = 0.2$, since the higher channel correlation causes interference strength more concentrated in few directions (see Fig. 4). A similar conclusion can be found for $\rho = 0.4$, and we omit the figure to conserve space. Clearly, the setting of rank threshold scaling factor η has different effect on different interference links in terms of effective rank determination.

Fig. 9 shows the total number of data streams in the network from our optimal objective (averaged over 10 random network instances similar to Fig. 7). As shown in this figure, for a given ρ , the total number of data streams steadily increases from 24 to 96 and then flattens out. This is because the higher the rank threshold scaling factor η , the lower the effective channel ranks on interference links in the network. As a result, fewer DoFs are needed to cancel interferences and more DoFs can be allocated for SM. When η is greater than 20, the number of data streams cannot be further increased, either there is no room to further decrease

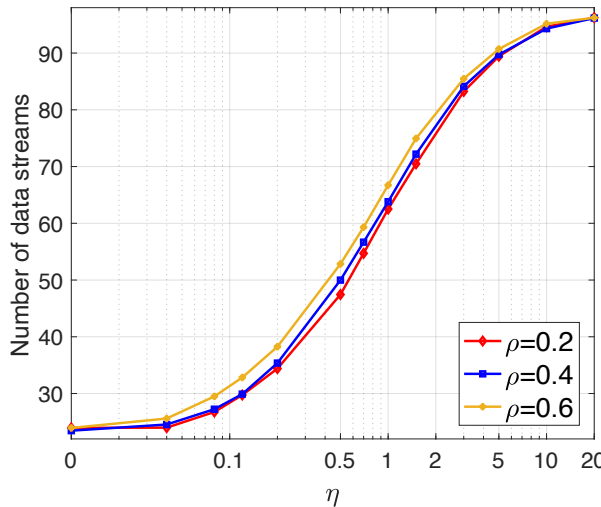


Fig. 9: Total number of data streams in the network.

of effective ranks on interference links (all effective ranks are 0), or further decrease of effective ranks on interference links will not improve objective value, due to the bounds on effective ranks on SM links. We also observe that for the same rank threshold η , a higher number of data streams can be achieved for higher channel correlation level, due to lower effective ranks.

The above example demonstrates the impact of effective rank threshold setting on the number of data streams that can be transported in the network. However, a larger number of data streams in the network does not necessarily mean a higher throughput, due to un-cancelled interference (considered as noise) and channel hardening effect [53]. In the next section, we investigate the impact of effective rank threshold setting on achievable throughput in the network.

5 THROUGHPUT CALCULATION AND OPTIMAL THROUGHPUT- η TRADE-OFF

This section presents our main results. We first calculate the actual throughput for a given DoF allocation for SM and IC. Then we show the trade-off between throughput maximization and interference threshold scaling factor η . To better demonstrate our main idea, we assume the Tx and Rx weights are already found for a given DoF allocation in this section. We will show one implementation on how to derive these weights in Section 6.

5.1 Throughput Calculation

Assume a DoF allocation for SM and IC is feasible for an MU-MIMO network. Then the network throughput is the sum of the throughput achieved on each data stream under SM. So the key question is how to calculate throughput for each SM stream.

For each data stream, we can calculate its throughput by finding its SINR and then apply the Shannon capacity formula. The only subtlety here is that the SINR calculation should include all interferences that this data stream is suffering from, which includes all un-cancelled interference at PHY layer and white noise. To do this, we need to go to the

PHY layer and work with the transmit and receive vectors for each data stream. Denote $\mathbf{U}_i \in \mathbb{C}^{N_i^T \times z_{i*}}$ as the weight matrix at Tx node i with z_{i*} outgoing SM data streams and $\mathbf{V}_j \in \mathbb{C}^{N_j^R \times z_{*j}}$ as the weight matrix at Rx node j with z_{*j} incoming SM data streams. Assume we have additive white Gaussian noise (AWGN) with zero mean and variance n_0^2 . To satisfy the transmit power constraint at node i and decoding power constraint at node j , the weight matrices must satisfy

$$\text{Tr}(\mathbf{U}_i \mathbf{U}_i^H) = 1, \quad \text{Tr}(\mathbf{V}_j \mathbf{V}_j^H) = 1, \quad (i \in \mathcal{K}^T, j \in \mathcal{K}^R).$$

In Section 6, we will show one implementation on how to derive \mathbf{U}_i and \mathbf{V}_j based on a DoF allocation while guaranteeing PHY layer feasibility. For now, let's assume the \mathbf{U}_i 's and \mathbf{V}_j 's are already found. Define the partition of matrix \mathbf{U}_i as $[\mathbf{U}_{i,j_1} \mathbf{U}_{i,j_2} \cdots \mathbf{U}_{i,j_M}]$, where j_1, j_2, \dots, j_M are Tx node i 's M recipients, i.e., $\{j_1, j_2, \dots, j_M\} = \mathcal{K}_i^R$, then $\mathbf{U}_{i,j_1}, \mathbf{U}_{i,j_2}, \dots, \mathbf{U}_{i,j_M}$ are sub-weights corresponding to Rx nodes j_1, j_2, \dots, j_M , with dimensions $N_i^T \times z_{ij_1}, N_i^T \times z_{ij_2}, \dots, N_i^T \times z_{ij_M}$ ($z_{i*} = \sum_{n=1}^M z_{ij_n}$), respectively.

For any $j \in \mathcal{K}_i^R$, the signal-to-interference-plus-noise ratio (SINR) of the f -th stream on link $i \rightarrow j$ is then given by

$$\text{SINR}_{ij}^f = \frac{\gamma_{ij}^f}{\mathbf{V}_j^{[*f]H} \mathbf{Q}_j \mathbf{V}_j^{[*f]} - \gamma_{ij}^f}, \quad (14)$$

where $(\cdot)^{[*f]}$ is the f -th column of (\cdot) and

$$\begin{aligned} \gamma_{ij}^f &= P_i L_{ij} \mathbf{V}_j^{[*f]H} \mathbf{H}_{ij}^H \mathbf{U}_{i,j}^{[*f]H} \mathbf{U}_{i,j}^{[*f]} \mathbf{H}_{ij} \mathbf{V}_j^{[*f]}, \\ \mathbf{Q}_j &= n_0^2 \mathbf{I}_{N_j} + \sum_{k \in \mathcal{K}^T} P_k L_{kj} \mathbf{H}_{kj}^H \mathbf{U}_k^H \mathbf{U}_k \mathbf{H}_{kj}. \end{aligned}$$

Finally, the network throughput (in bits/s) is given by

$$C = W_0 \sum_{i \in \mathcal{K}^T} \sum_{j \in \mathcal{K}_i^R} \sum_{f=1}^{z_{ij}} \log_2 (1 + \text{SINR}_{ij}^f), \quad (15)$$

where W_0 is the bandwidth.

5.2 Optimal Throughput- η Trade-off

From the network throughput expression (15), it is evident that there exists a trade-off between throughput and η . When η increases, more DoFs will be made available to support a larger number of SM data streams z_{ij} (as shown in Section 4) and we have a larger value of z_{ij} in (15) to increase throughput. On the other hand, higher η means more weak interferences are not cancelled and left in the network. This will decrease the SINR term in (15) and decrease throughput. Thus, we have a trade-off. Unfortunately, due to the non-convex nature of (15), a closed-form expression to explore optimal throughput- η trade-off remains unknown. In the rest of this section, we use simulation study to explore an optimal throughput- η trade-off and gain insights.

We use the same MU-MIMO network setting in Section 4.2. We randomly generate 10 instances and evaluate the average performance among the 10 instances. Fig. 10 shows network throughput vs. η under different channel correlation levels ρ . Note that $\eta = 0$ stands for traditional DoF IC that uses DoFs to cancel interference indiscriminately in all directions in the eigenspace. For $\rho = 0.2$, we can see network throughput keep increasing until threshold

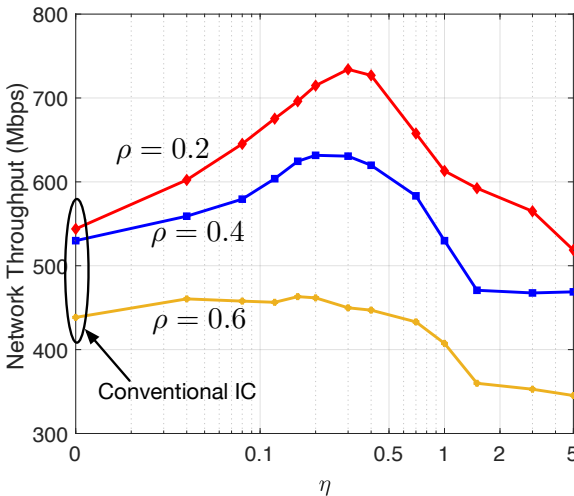
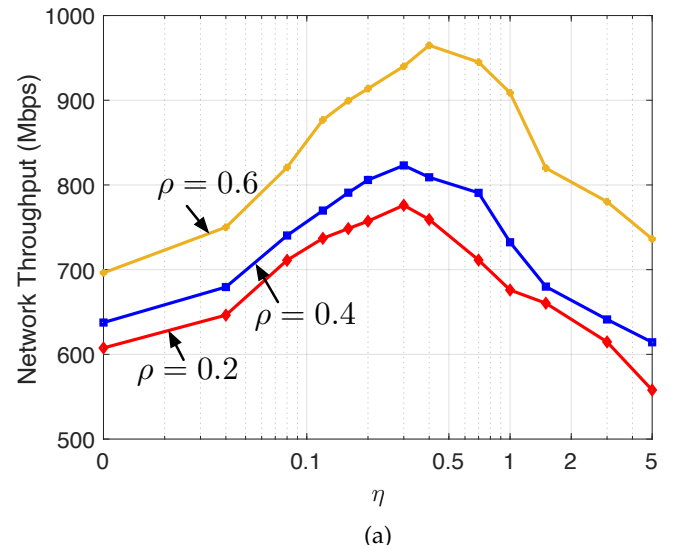


Fig. 10: Performance of network throughput under increasing threshold η . Kronecker model for both intended and interference channels.

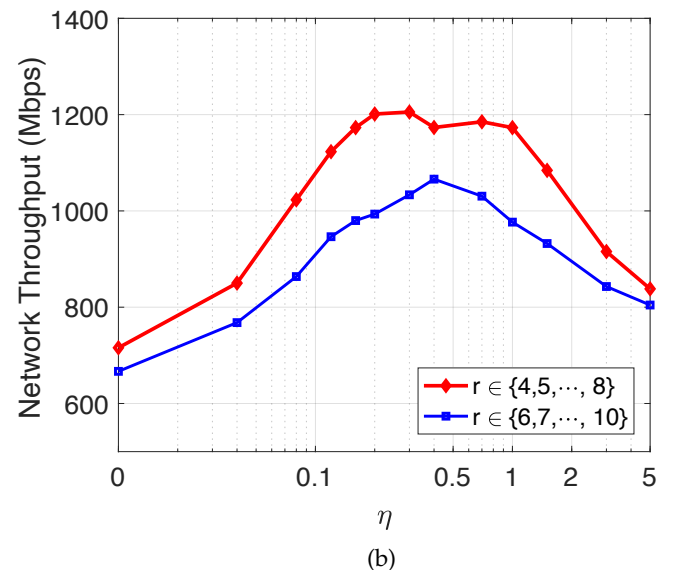
$\eta = 0.3$, as more data streams are supported (see Fig. 9) while weak (un-cancelled) interference has negligible impact (Section 6 will show the interference level versus η). However, as we further increase η , throughput decreases due to un-cancelled interference. Throughput under $\eta = 3$ can be as good as that with traditional IC (i.e., $\eta = 0$). By increasing η larger than 3, even though more DoFs can be made available for SM, un-cancelled interference will play a dominant role and will result in worse performance than traditional IC. For $\rho = 0.4$ and 0.6, we can see a similar trade-off. For this network setting, the optimal effective rank threshold η should be set to $\eta = 0.3, 0.2$ and 0.16 for $\rho = 0.2, 0.4$ and 0.6, respectively. The peak throughput (achieved at optimal η) is 34.9%, 19.2%, 5.6% more than that achieved at $\eta = 0$ for $\rho = 0.2, 0.4$ and 0.6, respectively. We also note that with a higher channel correlation level ρ , network throughput becomes lower. This is because high channel correlation also hinders MIMO's SM capability, which results in a lower throughput performance.

In the scenarios where intended links present low correlations while interference links present high correlations (e.g., high correlation caused by poor scattering or "key-hole" effect [38, 39]), our rank-based IC can be even more beneficial. To demonstrate this, we consider two different scenarios. First, fast fading for intended links is modeled by Rayleigh channel while fast fading for interference links is modeled by Kronecker model. Second, fast fading for intended links is modeled by Rayleigh channel while fast fading for interference links is modeled by reduced-rank model [54–56].

For Fig. 11(a), fast fading for intended links is modeled by Rayleigh channel, i.e., $\mathbf{H}_{ij} = \mathbf{H}_w$ ($i \in \mathcal{K}^T, j \in \mathcal{K}_i^R$), while fast fading for interference links is modeled by $\mathbf{H}_{ij} = \mathbf{R}_{tx}^{1/2} \mathbf{H}_w \mathbf{R}_{rx}^{1/2}$ ($i \in \mathcal{K}^T, j \in \mathcal{K}^R, j \notin \mathcal{K}_i^R$), with $\rho \in \{0.4, 0.6, 0.8\}$. As shown in Fig. 11(a), network throughput follows a similar trend as Fig. 10 as we increase effective rank threshold η . However, we observe that for a higher channel correlation level ρ at interference links, we



(a)



(b)

Fig. 11: Performance of network throughput under increasing threshold η . (a) Kronecker model for interference channels and Rayleigh model for intended channels. (b) Rank-reduced channel model for interference channels and Rayleigh model for intended channels.

obtain a much higher throughput gain by setting optimal effective rank threshold η . Specifically, the peak throughput (achieved at optimal η) is 27.7%, 29.1%, 38.6% more than that achieved at $\eta = 0$ for $\rho = 0.4, 0.6$ and 0.8, respectively. This is because well-conditioned intended channels have the capability to achieve higher throughput when carrying more data streams, thus can fully benefit from exploiting interference signal strength in the eigenspace on correlated interference channels.

Different from Fig. 11(a), Fig. 11(b) shows the results that fast fading for intended links is still modeled by Rayleigh channel while interference links are modeled by reduced-rank channel model [54, 55]. Reduced-rank channel model generates channels by letting $\mathbf{H}_{ij} = \mathbf{AB}$, where \mathbf{A} is an $N_i^T \times r$ full-rank matrix with its entries containing zero-mean i.i.d. complex Gaussian random variables, and \mathbf{B} is a $r \times N_j^R$ full-

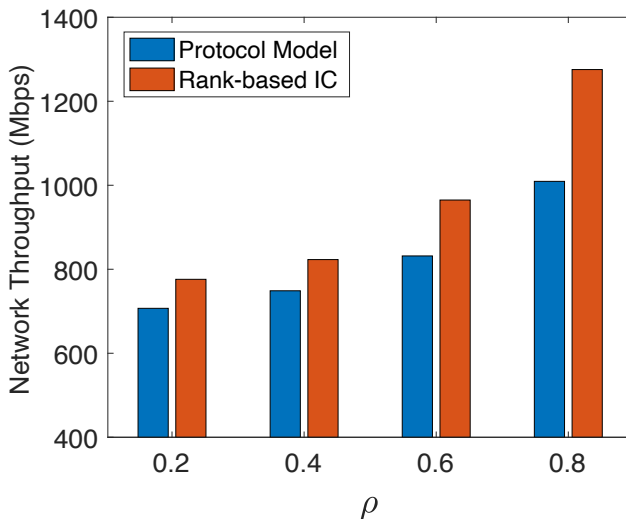


Fig. 12: Comparison of network throughput achieved by rank-based IC and protocol model-based IC.

rank rectangular unitary matrix, where $r \leq \min\{N_i^T, N_j^R\}$. This model can guarantee that the channel is of rank r (with probability 1). In our simulation experiment, the rank of an interference channel r is randomly chosen from $\{4, 5, \dots, 8\}$ and $\{6, 7, \dots, 10\}$, respectively. Fig. 11(b) also presents the throughput- η trade-off. We observe that the highest network throughput is 68.4% and 59.8% more than that achieved at $\eta = 0$ for $r \in \{4, 5, \dots, 8\}$ and $r \in \{6, 7, \dots, 10\}$, respectively. The trade-off in Fig. 10 and 11 reaffirms that blind IC in all its directions is not efficient from a throughput perspective.

In Fig. 12, we compare the throughput performance of our rank-based IC with protocol model-based IC. Under the protocol model (or disc model), an Rx node within a predefined interference range is considered interfered and IC is required for these Rx nodes, while an Rx node outside that range does not require IC. Protocol model-based IC is solely based on distance, regardless of the interference strength in different directions on a MIMO channel. Fig. 12 shows the throughput performance under protocol model-based IC with the interference range of 500 m, and the throughput achieved by our IC scheme. The results suggest that the network throughput by our IC scheme is 9.7%, 9.9%, 16.1% and 26.4% more than that achieved by protocol model-based IC for $\rho = 0.2, 0.4, 0.6$ and 0.8, respectively.

6 PHYSICAL LAYER FEASIBILITY

In Section 5 we assumed feasible weight matrices \mathbf{U}_i and \mathbf{V}_j at the PHY layer are given *a priori* corresponding to a particular DoF allocation. In this section, we show how to find such weight matrices at each node.

As expected, finding these feasible at the PHY layer for an MU-MIMO network is not trivial. First and foremost, the Tx weights and Rx weights are interdependent on each other. That is, the Tx weights for IC depend on the corresponding Rx weights, while the Rx weights for IC also depend on the corresponding Tx weights. There is no established guideline in the literature on how to find feasible weight matrices corresponding to a DoF allocation such that interference can be cancelled completely. Second, since we are

exploring effective channel ranks in this paper and some weak interferences are not cancelled by DoFs, one cannot guarantee the existence of feasible \mathbf{U}_i and \mathbf{V}_j to achieve perfect (100%) interference-free transmission. This makes finding feasible weight matrices even more challenging.

Inspired by the weights design in [23, 24], we propose an iterative algorithm that is able to set the weights based on the DoF solution for a specific objective as shown in Section 4. Different from the designs in [23, 24], our algorithm focused on cancelling the strong interferences in best rank- r channels based on given DoF allocations from Section 4. The goal is to have remaining signal strength in the directions of strong interferences close to zero.

6.1 Basic Idea

The main idea of our algorithm is as follows. For a given DoF allocation, we have the data stream allocation (i.e. z_{ij}) on each SM link in the network, which we can use to determine the dimension for each \mathbf{U}_i and \mathbf{V}_j . Then, under the original channel matrix \mathbf{H}_{ij} , to cancel all the inter-stream and inter-node interference, we must have

$$\mathbf{U}_i^H [\mathbf{H}_{ij_1} \mathbf{V}_{j_1} \ \mathbf{H}_{ij_2} \mathbf{V}_{j_2} \dots] = \Lambda_{z_{i*}}, \quad i \in \mathcal{K}^T, j_1, j_2, \dots \in \mathcal{K}_i^R, \quad (16)$$

$$\mathbf{U}_i^H \mathbf{H}_{ij} \mathbf{V}_j = \mathbf{0}, \quad i \in \mathcal{K}^T, j \in \mathcal{K}^R, j \notin \mathcal{K}_i^R, \quad (17)$$

where $\Lambda_{z_{i*}}$ is a $z_{i*} \times z_{i*}$ diagonal matrix with z_{i*} non-zero diagonal elements.

Although (16) can always be satisfied for all SM links by standard ZF design, (17), however, cannot be satisfied for all $i \in \mathcal{K}^T, j \in \mathcal{K}^R, j \notin \mathcal{K}_i^R$ if there are not enough remaining DoFs to cancel those weak interference on some links. Recognizing that not all interference can be perfectly cancelled, we focus our goal on cancelling all the strong interference, which is based on the best rank- r approximate channel $\tilde{\mathbf{H}}_{ij} = \sum_{l=1}^{r_{ij}} \sigma_l \mathbf{u}_l \mathbf{v}_l^H$ via SVD of \mathbf{H}_{ij} . That is, we want to have

$$\mathbf{U}_i^H \tilde{\mathbf{H}}_{ij} \mathbf{V}_j = \mathbf{0}, \quad \text{for } i \in \mathcal{K}^T, j \in \mathcal{K}^R, j \notin \mathcal{K}_i^R. \quad (18)$$

The weak (un-cancelled) interference will reduce network throughput and will be taken into account in throughput calculation (as we did in Section 5).

Equations (16) and (18) constitute a system of bilinear equations and a general solution to bilinear equations remains unknown [57]. Instead of finding a feasible solution to (16) and (18), we propose to minimize the LHS of (18) for all $i \in \mathcal{K}^T, j \in \mathcal{K}^R, j \notin \mathcal{K}_i^R$, subject to (16). Denote \mathcal{A}_{LI} as the leakage interference in the network,³ which is defined as

$$\mathcal{A}_{LI} = \sum_{i \in \mathcal{K}^T} \sum_{j \in \mathcal{K}^R} P_i L_{ij} \left\| \mathbf{U}_i^H \tilde{\mathbf{H}}_{ij} \mathbf{V}_j \right\|_F^2. \quad (19)$$

The problem to solve is to minimize \mathcal{A}_{LI} subject to (16).

To do this, we propose a simple yet effective approach to address the dependency between Tx weight matrices \mathbf{U}_i and Rx weight matrices \mathbf{V}_j by updating each in an alternating fashion (i.e., fixing \mathbf{U}_i and update \mathbf{V}_j and vice versa). Specifically, in each iteration, Tx weight matrices \mathbf{U}_i are optimized first with given Rx weight matrices \mathbf{V}_j and

3. A similar definition of leakage interference involving only channel matrix \mathbf{H}_{ij} is given in [23, 24].

channel information. Then we optimize Rx weight matrices \mathbf{V}_j with given Tx weight matrices \mathbf{U}_i and channel information. For each weight matrix (either at Tx or Rx node) optimization, the weight matrix is updated by solving a minimization problem with the objective \mathcal{J}_{LI} and the updated set of constraints. The iteration terminates if we find no improvement after a number of consecutive iterations.

6.2 Algorithm Details

Now we describe in detail on how to find weight matrices.

Step 1: Initialization. Initially all the Tx and Rx weight matrices can be set arbitrarily but have to be full rank matrices with dimension $N_i^T \times z_{i*}$ and $N_j^R \times z_{*j}$, respectively.

Step 2: Optimizing Tx Weights. In this step, channel information $\tilde{\mathbf{H}}_{ij}$ and Rx weight matrices \mathbf{V}_j are given. We optimize Tx weight matrices \mathbf{U}_i so as to minimize leakage interference. Denote $\mathcal{J}_{\text{LI},i}^T = \sum_{j \in \mathcal{K}^R} P_i L_{ij} \|\mathbf{U}_i^H \tilde{\mathbf{H}}_{ij} \mathbf{V}_j\|_F^2$ as the leakage interference at Tx node i , then

$$\min_{\mathbf{U}_1, \mathbf{U}_2, \dots, \mathbf{U}_{|\mathcal{K}^T|}} \mathcal{J}_{\text{LI}} = \min_{\mathbf{U}_1, \mathbf{U}_2, \dots, \mathbf{U}_{|\mathcal{K}^T|}} \sum_{i \in \mathcal{K}^T} \mathcal{J}_{\text{LI},i}^T = \sum_{i \in \mathcal{K}^T} \min_{\mathbf{U}_i} \mathcal{J}_{\text{LI},i}^T. \quad (20)$$

It follows that $\min \mathcal{J}_{\text{LI}}$ can be solved separately by solving $|\mathcal{K}^T|$ independent sub-problems $\min_{\mathbf{U}_i} \mathcal{J}_{\text{LI},i}^T$, i.e., one subproblem for each Tx node. (Note that $\mathcal{J}_{\text{LI}} = \sum_{i \in \mathcal{K}^T} \mathcal{J}_{\text{LI},i}^T$ and $\mathcal{J}_{\text{LI},i}^T$'s are independent among each other). The constraints of sub-problem i are based on Tx node i 's IC responsibilities (i.e., the number of DoFs needed to cancel interference from i to j at Tx node i (d_{ij}^T) per our discussion in Section 4). For Tx node i (sub-problem i), we have the following three cases to determine the sets of constraints to optimize \mathbf{U}_i :

- $d_{ij}^T = 0, j \in \mathcal{K}^R$. In this case, Tx node i is not responsible for cancelling interference from Tx node i to Rx node j . Thus no constraint is needed in this case.
- $d_{ij}^T = z_{*j}$ and $d_{ij}^T < r_{ij}, j \in \mathcal{K}^R$. In this case, Tx node i is responsible for cancelling all the interference from Tx node i to Rx node j . Denote \mathcal{D}_i^T as the set of Rx nodes that Tx node i is responsible for cancelling all its interference, i.e., $\mathcal{D}_i^T = \{j : d_{ij}^T = z_{*j}, d_{ij}^T < r_{ij}, j \in \mathcal{K}^R, j \notin \mathcal{K}_i^R\}$. Then the following set of constraints is needed for optimizing \mathbf{U}_i :

$$\mathbf{U}_i^H \tilde{\mathbf{H}}_{ij} \mathbf{V}_j = \mathbf{0}, \quad j \in \mathcal{D}_i^T, i \in \mathcal{K}^T.$$

- $d_{ij}^T < z_{*j}$ or $d_{ij}^T = r_{ij}, j \in \mathcal{K}^R$. In this case, the number of DoFs consumed to cancel interference from Tx node i to Rx node j is shared between nodes i and j . That is, Tx node i uses d_{ij}^T DoFs to cancel interferences from d_{ij}^T directions in the eigenspace, and the remaining interferences (from $d_{ij}^R = r_{ij} - d_{ij}^T$ directions in the eigenspace) will be cancelled by Rx node j (when optimizing Rx weights later in Step 3), which guarantees the interference channel (based on best rank- r approximation) is cleared for data transmission. Note that in this case Rx weight matrix \mathbf{V}_j is not needed in the constraints to update \mathbf{U}_i ; only the channel matrix $\tilde{\mathbf{H}}_{ij}$ is needed. Let $\tilde{\mathbf{H}}_{ij}^{[m,n]} = \sum_{l=m}^n \sigma_l \mathbf{u}_l \mathbf{v}_l^H$ which represents the channel information at directions corresponding to the m -th

to the n -th largest eigenvalues (recall that the SVD of \mathbf{H}_{ij} is $\mathbf{H}_{ij} = \sum_{l=1}^{N_i^R} \sigma_l \mathbf{u}_l \mathbf{v}_l^H$). Denote $\tilde{\mathcal{D}}_i^T = \{j : 0 < d_{ij}^T < z_{*j} \text{ or } d_{ij}^T = r_{ij}, j \in \mathcal{K}^R, j \notin \mathcal{K}_i^R\}$ as the set of Rx nodes that Tx node i is partially responsible for cancelling its interference. Then we have the following set of constraints:

$$\tilde{\mathbf{H}}_{ij}^{[1,d_{ij}^T]H} \mathbf{U}_i = \mathbf{0}, \quad j \in \tilde{\mathcal{D}}_i^T, i \in \mathcal{K}^T.$$

In addition, as a necessary condition to distinguish different data streams, Tx weight matrix \mathbf{U}_i must have linearly independent columns. We consider the following constraint to guarantee the independency among the columns of \mathbf{U}_i :

$$\mathbf{U}_i^H \mathbf{U}_i = \frac{1}{z_{i*}} \mathbf{I}.$$

Putting together the objective function and all the constraints above, for each Tx node $i \in \mathcal{K}^T$, we have the following optimization problem for Tx weight matrix \mathbf{U}_i :

$$\begin{aligned} \text{OPT-Tx-}i \quad \min_{\mathbf{U}_i \in \mathbb{C}^{N_i^T \times z_{i*}}} \mathcal{J}_{\text{LI},i}^T &= \sum_{j \in \mathcal{K}^R} P_i L_{ij} \|\mathbf{U}_i^H \tilde{\mathbf{H}}_{ij} \mathbf{V}_j\|_F^2, \\ \text{s.t.} \quad \mathbf{U}_i^H \mathbf{U}_i &= \frac{1}{z_{i*}} \mathbf{I}, \\ \mathbf{V}_j^H \tilde{\mathbf{H}}_{ij}^H \mathbf{U}_i &= \mathbf{0}, \quad j \in \mathcal{D}_i^T, \\ \tilde{\mathbf{H}}_{ij}^{[1,d_{ij}^T]H} \mathbf{U}_i &= \mathbf{0}, \quad j \in \tilde{\mathcal{D}}_i^T. \end{aligned}$$

where $\mathcal{D}_i^T = \{j : d_{ij}^T = z_{i*}, d_{ij}^T < r_{ij}, j \in \mathcal{K}^R\}$, $\tilde{\mathcal{D}}_i^T = \{j : d_{ij}^T < z_{i*} \text{ or } d_{ij}^T = r_{ij}, j \in \mathcal{K}^R\}$ and $\tilde{\mathbf{H}}_{ij}^{[m,n]} = \sum_{l=m}^n \sigma_l \mathbf{u}_l \mathbf{v}_l^H$.

The optimal solution to problem OPT-Tx- i is given by the following lemma.

Lemma 1 *The optimal solution to problem OPT-Tx- i is*

$$\mathbf{U}_i = \begin{cases} \frac{1}{\sqrt{z_{i*}}} \cdot \text{nullspace}^{[1,z_{i*}]} \left(\begin{bmatrix} \mathbf{B} \mathbf{A} \mathbf{B} \\ \mathbf{C} \end{bmatrix} \right), & \text{if } z_{i*} \leq N_i^T - c \\ \frac{1}{\sqrt{z_{i*}}} \cdot \left[\text{nullspace} \left(\begin{bmatrix} \mathbf{B} \mathbf{A} \mathbf{B} \\ \mathbf{C} \end{bmatrix} \right) \text{ eig}^{[N_i^T-p+1, z_{i*}+c-p]} (\mathbf{B} \mathbf{A} \mathbf{B}) \right], & \text{if } z_{i*} > N_i^T - c \end{cases}$$

where $\mathbf{B} \mathbf{A} \mathbf{B}$ is a matrix from the matrix multiplication of \mathbf{B} by \mathbf{A} by \mathbf{B} , $\begin{bmatrix} \mathbf{B} \mathbf{A} \mathbf{B} \\ \mathbf{C} \end{bmatrix}$ is a vertical stack of matrices $\mathbf{B} \mathbf{A} \mathbf{B}$ and \mathbf{C} , $p = \text{rank}(\mathbf{B} \mathbf{A} \mathbf{B})$, $c = \text{rank}([\mathbf{B} \mathbf{A} \mathbf{B}])$, $\mathbf{A} = \sum_{j \notin \mathcal{K}^R} P_j L_{ij} \tilde{\mathbf{H}}_{ij} \mathbf{V}_j \mathbf{V}_j^H \tilde{\mathbf{H}}_{ij}^H$, \mathbf{B} is a projection matrix given by $\mathbf{B} = \mathbf{I}_{z_{i*}} - \mathbf{C}^H (\mathbf{C} \mathbf{C}^H)^{-1} \mathbf{C}$, and \mathbf{C} is given by

$$\mathbf{C} = \begin{bmatrix} \mathbf{V}_{\bar{j}_1}^H \tilde{\mathbf{H}}_{i\bar{j}_1}^H \\ \mathbf{V}_{\bar{j}_2}^H \tilde{\mathbf{H}}_{i\bar{j}_2}^H \\ \vdots \\ \tilde{\mathbf{H}}_{i\hat{j}_1}^{[1,d_{ij_1}^T]H} \\ \tilde{\mathbf{H}}_{i\hat{j}_2}^{[1,d_{ij_2}^T]H} \\ \vdots \end{bmatrix} \quad \text{with } \{\bar{j}_1, \bar{j}_2, \dots\} = \mathcal{D}_i^T, \quad \{\hat{j}_1, \hat{j}_2, \dots\} = \tilde{\mathcal{D}}_i^T,$$

and $\text{nullspace}^{[1,z_{i*}]}(\mathbf{X})$ denotes z_{i*} orthonormal vectors in the nullspace of \mathbf{X} , and $\text{eig}^{[a,b]}(\mathbf{X})$ is the eigenvectors of \mathbf{X} corresponding to the a -th smallest to the b -th smallest eigenvalues. Further, the optimal objective value is given by

$$\frac{1}{z_{i*}} \cdot \sum_{l=c-p+1}^{z_{i*}+c-p} \lambda_l(\mathbf{B} \mathbf{A} \mathbf{B}).$$

where $\lambda_l(\mathbf{X})$ is the l -th smallest eigenvalue of matrix \mathbf{X} .

A proof of Lemma 1 is given in Appendix ??.

To ensure our algorithm to converge, we let \mathbf{U}_i be updated only when the current optimal objective value is smaller than that in the last iteration, i.e., $\mathcal{A}_{\text{LI},i}^T(t) < \mathcal{A}_{\text{LI},i}^T(t-1)$. Otherwise \mathbf{U}_i remains unchanged as in the last iteration until updates in future iterations.

Step 3: Optimizing Rx Weights. Similar to optimizing Tx weight matrices, we have $|\mathcal{K}^R|$ independent sub-problems for $|\mathcal{K}^R|$ Rx nodes, and each has three sets of constraints to optimize Rx weight matrix \mathbf{V}_j . Deriving these constraints is similar to Step 2. Then the optimization problem for Rx weight matrix \mathbf{V}_j is:

$$\begin{aligned} \text{OPT-Rx-}j \quad \min_{\mathbf{V}_j \in \mathbb{C}^{N_j^R \times z_{*j}}} \quad & \mathcal{A}_{\text{LI},j}^R = \sum_{i \in \mathcal{K}^T}^{i \neq s(j)} P_i L_{ij} \|\mathbf{U}_i^H \tilde{\mathbf{H}}_{ij} \mathbf{V}_j\|_F^2, \\ \text{s.t.} \quad & \mathbf{V}_j^H \mathbf{V}_j = \frac{1}{z_{*j}} \mathbf{I}, \\ & \mathbf{U}_i^H \tilde{\mathbf{H}}_{ij} \mathbf{V}_j = \mathbf{0}, \quad i \in \mathcal{D}_j^R, \\ & \tilde{\mathbf{H}}_{ij}^{[d_{ij}^T+1, r_{ij}]} \mathbf{V}_j = \mathbf{0}, \quad i \in \tilde{\mathcal{D}}_j^R, \end{aligned}$$

where $\mathcal{D}_j^R = \{i : d_{ij}^R = z_{*j}, d_{ij}^R < r_{ij}, i \in \mathcal{K}^T, j \notin \mathcal{K}_i^R\}$ and $\tilde{\mathcal{D}}_j^R = \{i : 0 < d_{ij}^R < z_{*j} \text{ or } d_{ij}^R = r_{ij}, i \in \mathcal{K}^T, j \notin \mathcal{K}_i^R\}$.

Solving problem OPT-Rx-j is similar to that for problem OPT-Tx-i and we omit the details to conserve space. To guarantee convergence, \mathbf{V}_j is updated only when current optimal objective value $\mathcal{A}_{\text{LI},j}^R(t)$ is smaller than $\mathcal{A}_{\text{LI},j}^R(t-1)$ of last iteration. Otherwise \mathbf{V}_j remains the same until updates in future iterations.

Step 2 and Step 3 are iteratively performed until there is no improvement for W consecutive iterations, i.e., $\mathcal{A}_{\text{LI}}(t-w-1) - \mathcal{A}_{\text{LI}}(t-w) < \epsilon, w = 0, 1, \dots, W-1$ is met for a given convergence threshold ϵ .

Step 4: Cancelling Intra-node Interference. Within an intended link, there may exist multiple data streams and they would also interfere with each other. In this step, we cancel such intra-node interference to decode the desired data streams. This can be done by performing a linear transformation of Tx weight \mathbf{U}_i by multiplying a matrix \mathbf{F}_i . Such a linear transformation can decode different intra-node data streams while not affecting inter-node IC.

To show how such a linear transformation works, let's denote

$$\mathbf{\Gamma}_i = [\mathbf{H}_{ij_1} \mathbf{V}_{j_1} \quad \mathbf{H}_{ij_2} \mathbf{V}_{j_2} \quad \cdots], \quad j_1, j_2, \dots \in \mathcal{K}_i^R, i \in \mathcal{K}^T.$$

Then we define \mathbf{F}_i as

$$\mathbf{F}_i = (\mathbf{U}_i^H \mathbf{\Gamma}_i)^{-1}, \quad i \in \mathcal{K}^T.$$

To perform a linear transformation on Tx weight matrix \mathbf{U}_i , we multiply it by matrix \mathbf{F}_i . We have:

$$\mathbf{U}_i \leftarrow \mathbf{U}_i \mathbf{F}_i^H, \quad i \in \mathcal{K}^T. \quad (21)$$

It is easy to verify that after such a transformation, we have $\mathbf{U}_i^H \mathbf{\Gamma}_i = \mathbf{I}_{z_{*i}}$.

Step 5: Power Allocation. We apply equal power allocation for each data stream, subject to the total power constraints $\text{Tr}(\mathbf{U}_i \mathbf{U}_i^H) = 1, \text{Tr}(\mathbf{V}_j \mathbf{V}_j^H) = 1$. We have

$$\begin{aligned} \mathbf{U}_i^{[*f]} &\leftarrow \frac{1}{\sqrt{z_{*i}}} \frac{\mathbf{U}_i^{[*f]}}{\|\mathbf{U}_i^{[*f]}\|}, \quad \forall i \in \mathcal{K}^T, f = 1, 2, \dots, z_{*i}, \\ \mathbf{V}_j^{[*f]} &\leftarrow \frac{1}{\sqrt{z_{*j}}} \frac{\mathbf{V}_j^{[*f]}}{\|\mathbf{V}_j^{[*f]}\|}, \quad \forall j \in \mathcal{K}^R, f = 1, 2, \dots, z_{*j}. \end{aligned} \quad (22)$$

A pseudocode of our proposed algorithm to compute Tx and Rx weights is given in Algorithm 1. A proof of the algorithm's convergence is given in Appendix ??.

Although Algorithm 1 minimizes leakage interference in each iteration and is proven to converge, the objective value upon this convergence may only be sub-optimal. Nevertheless, we find that this algorithm is computationally efficient. The performance of the algorithm is presented in the following section.

Algorithm 1: Computing Tx and Rx Weights

```

input :  $\mathbf{H}_{ij}, r_{ij}, z_{ij}, d_{ij}^R, d_{ij}^T, P_i, L_{ij}$ 
output :  $\mathbf{U}_i, \mathbf{V}_j$ 
parameter:  $\epsilon, W$ 

1 Initialize: Start with arbitrary weight matrices:
2    $\mathbf{U}_i: N_i^T \times z_{*i}, \text{rank}(\mathbf{U}_i) = z_{*i};$ 
3    $\mathbf{V}_j: N_j^R \times z_{*j}, \text{rank}(\mathbf{V}_j) = z_{*j};$ 
4    $\text{NonImproveIter} = 0;$ 
5 while  $\text{NonImproveIter} < W$ , do
6   foreach  $i \in \mathcal{K}^T$  do
7     Solve optimization Problem OPT-Tx-i ;
8     if  $\mathcal{A}_{\text{LI},i}^T(t) < \mathcal{A}_{\text{LI},i}^T(t-1)$  then
9       |  $\mathbf{U}_i \leftarrow$  solution to Problem OPT-Tx-i ;
10      end
11    end
12   foreach  $j \in \mathcal{K}^R$  do
13     Solve optimization Problem OPT-Rx-j ;
14     if  $\mathcal{A}_{\text{LI},j}^R(t) < \mathcal{A}_{\text{LI},j}^R(t-1)$  then
15       |  $\mathbf{V}_j \leftarrow$  solution to Problem OPT-Rx-j ;
16     end
17   end
18   if  $\mathcal{A}_{\text{LI}}(t-1) - \mathcal{A}_{\text{LI}}(t) < \epsilon$  then
19     |  $\text{NonImproveIter} \leftarrow \text{NonImproveIter} + 1$  ;
20   else
21     |  $\text{NonImproveIter} = 0$  ;
22   end
23 end
24 foreach  $j \in \mathcal{K}^R, i \in \mathcal{K}^T$  do
25   |  $\mathbf{U}_i \leftarrow$  performing linear transformation by (21) ;
26   |  $\mathbf{V}_j, \mathbf{U}_i \leftarrow$  performing equal power allocation
27   | by (22) ;
27 end

```

6.3 Performance

In this section, we examine the effectiveness of Algorithm 1 in terms of cancelling the strong interference. For evaluation, we first introduce the metric of *normalized residual interference*, which is defined as the ratio of residual interference

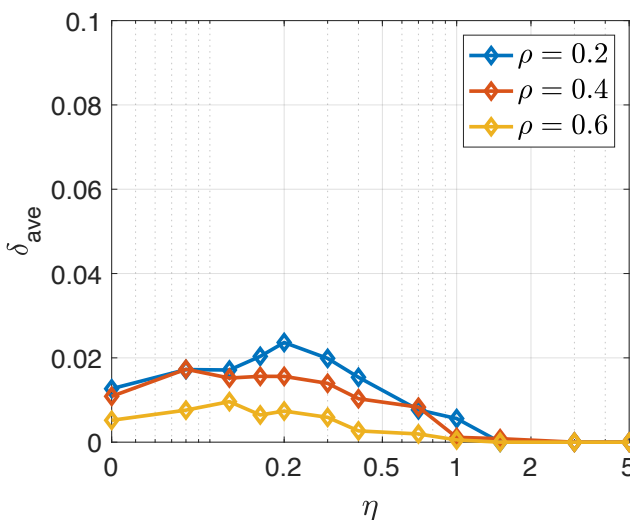


Fig. 13: The average normalized residual interference under different rank thresholds.

(i.e., the remaining portion of the strong interference after applying the weights at the PHY layer for IC) to the interference power before this IC.

Recall that $\tilde{\mathbf{H}}_{ij}$ is the best rank- r approximate of channel \mathbf{H}_{ij} (defined in Section 6.1). After applying the Tx and Rx weights found by Algorithm 1, the residual interference power perceived at Rx node j is $\sum_{i \in \mathcal{K}^T}^{i \neq s(j)} P_i L_{ij} \|\mathbf{U}_i^H \tilde{\mathbf{H}}_{ij} \mathbf{V}_j\|_F^2$, which we hope to be close to 0 (if our Algorithm 1 is effective). The interference power before IC can be expressed as $\sum_{i \in \mathcal{K}^T}^{i \neq s(j)} \frac{P_i}{N_i^T} L_{ij} \|\mathbf{H}_{ij}\|_F^2$. Then the normalized residual interference at Rx node j , denoted as $\tilde{\delta}_j$, is

$$\tilde{\delta}_j = \frac{\sum_{i \in \mathcal{K}^T}^{i \neq s(j)} P_i L_{ij} \|\mathbf{U}_i^H \tilde{\mathbf{H}}_{ij} \mathbf{V}_j\|_F^2}{\sum_{i \in \mathcal{K}^T}^{i \neq s(j)} \frac{P_i}{N_i^T} L_{ij} \|\mathbf{H}_{ij}\|_F^2}.$$

Denote δ_{ave} as the average normalized residual interference over all Rx nodes. Then δ_{ave} is given by

$$\delta_{ave} = \frac{1}{|\mathcal{K}^R|} \sum_{j \in \mathcal{K}^R} \tilde{\delta}_j.$$

We will use δ_{ave} as the primary performance metric to show the effectiveness of Algorithm 1.

We consider the same network setting as in Section 5. For the parameters of Algorithm 1, we set $\epsilon = 10^{-4}$ and $W = 5$. Fig. 13 shows that, by applying Algorithm 1, the average normalized residual interference is close to zero (less than 0.025) under all different network settings ($\rho = 0.2, 0.4$ and 0.6) and different effective rank thresholds. This demonstrates that the Tx and RX weights assigned by Algorithm 1 can successfully suppress the strong interference close to zero in all cases. That is, for practical purpose, Algorithm 1 can guarantee feasibility at the PHY layer for a given DoF allocation by the DoF IC model in Section 4.

7 CONCLUSIONS

In this paper, we developed a novel DoF IC strategy that exploited interference signal strengths among different directions in the eigenspace. By decomposing an interference

channel in its eigenspace and introducing an effective rank threshold to differentiate strong and weak interference, we showed that precious DoFs can be conserved if we only use DoFs to cancel those strong interference signals in the eigenspace. We investigated the trade-off between network throughput and effective rank threshold and showed that network throughput under the optimal effective rank threshold is significantly higher than that under existing DoF IC models. To ensure the new DoF IC model is feasible at the PHY layer, we proposed an algorithm to find the Tx and Rx weights such that the strong interferences beyond the effective rank threshold can be suppressed close to zero.

ACKNOWLEDGMENTS

This research was supported in part by NSF under grant CNS-1617634, Virginia Commonwealth Cyber Initiative (CCI), and Virginia Tech Institute for Critical Technology and Applied Science (ICTAS).

REFERENCES

- [1] Y. Chen, S. Li, C. Li, Y.T. Hou and B. Jalaian, "To cancel or not to cancel: Exploiting interference signal strength in the eigenspace for efficient MIMO DoF utilization," in *Proc. of IEEE INFOCOM*, pp. 1954–1962, Paris, France, April 29–May 2, 2019.
- [2] D.M. Blough, G. Resta, P. Santi, R. Srinivasan and L. M. Cortés-Pena, "Optimal one-shot scheduling for MIMO networks," in *Proc. of IEEE SECON*, pp. 404–412, Salt Lake City, UT, USA, June 2011.
- [3] Y. Shi, J. Liu, C. Jiang, C. Gao and Y.T. Hou, "A DoF-based link layer model for multi-hop MIMO networks," *IEEE Transactions on Mobile Computing*, vol. 13, no. 7, pp. 1395–1408, July 2014.
- [4] B. Hamdaoui and K.G. Shin, "Characterization and analysis of multi-hop wireless MIMO network throughput," in *Proc. of ACM MobiHoc*, pp. 120–129, Montreal, Quebec, Canada, Sept. 2007.
- [5] R. Bhatia and L. Li, "Throughput optimization of wireless mesh networks with MIMO links," in *Proc. of IEEE INFOCOM*, pp. 2326–2330, Barcelona, Spain, May 2007.
- [6] H. Yu, O. Bejarano and L. Zhong, "Combating inter-cell interference in 802.11ac-based multi-user MIMO networks," in *Proc. of ACM MobiCom*, pp. 141–152, Maui, Hawaii, USA, Sept. 2014.
- [7] D.M. Blough, P. Santi and R. Srinivasan, "On the feasibility of unilateral interference cancellation in MIMO networks," *IEEE/ACM Transactions on Networking*, vol. 22, no. 6, pp. 1831–1844, Dec. 2014.
- [8] K. Sundaresan, R. Sivakumar, M.A. Ingram and C. Tae-Young, "Medium access control in ad hoc networks with MIMO links: Optimization considerations and algorithms," *IEEE Transactions on Mobile Computing*, vol. 3, no. 4, pp. 350–365, Oct. 2004.
- [9] H. Zeng, Y. Shi, Y.T. Hou, R. Zhu and W. Lou, "A novel MIMO DoF model for multi-hop networks," *IEEE Network*, vol. 28, no. 5, pp. 81–85, Sept. 2014.
- [10] X. Xie, X. Zhang and E. Chai, "Cross-cell DoF distribution: combating channel hardening effect in multi-cell MU-MIMO networks," in *Proc. of ACM MobiHoc*, pp. 337–346 Hangzhou, China, June 2015.
- [11] S. Kumar, D. Cifuentes, S. Gollakota and D. Katabi, "Bringing cross-layer MIMO to today's wireless LANs," in *Proc. of ACM SIGCOMM*, Hong Kong, China, vol. 43, no. 4, pp. 387–398, Aug. 2013.
- [12] J.S. Park, A. Nandan, M. Gerla and L. Heechoon, "SPACE-MAC: Enabling spatial reuse using MIMO channel-aware MAC," in *Proc. of IEEE ICC*, pp. 3642–3646, Seoul, South Korea, May 2005.
- [13] J.C. Mundarath, P. Ramanathan and B.D. Van Veen, "Exploiting spatial multiplexing and reuse in multi-antenna wireless ad hoc networks," *Elsevier Ad Hoc Networks*, vol. 7, no. 2, pp. 281–293, March 2009.
- [14] R.H. Etkin, N.C. David and H. Wang, "Gaussian interference channel capacity to within one bit," *IEEE Transactions on Information Theory*, vol. 54, no. 12, pp. 5534–5562, Dec. 2008.

- [15] F. Negro, S.P. Shenoy, I. Ghauri and D.T. Slock, "On the MIMO interference channel", in *Proc. of IEEE Information Theory and Applications Workshop*, pp. 1–9, San Diego, CA, USA, Jan. 2010.
- [16] A. Host-Madsen and A. Nosratinia, "The multiplexing gain of networks," in *Proc. of IEEE ISIT*, pp. 2065–2069, Adelaide, Australia, Sept. 2005.
- [17] Q.H. Spencer, A.L. Swindlehurst and M. Haardt, "Zero-forcing methods for downlink spatial multiplexing in multiuser MIMO channels," *IEEE Transactions on Signal Processing*, vol. 52, no. 2, pp. 461–471, Feb. 2004.
- [18] L. Zheng and D.N.C. Tse, "Diversity and multiplexing: A fundamental tradeoff in multiple-antenna channels," *IEEE Transactions on Information Theory*, vol. 49, no. 5, pp. 1073–1096, May 2003.
- [19] H. Xie, F. Gao and S. Jin, "An overview of low-rank channel estimation for massive MIMO systems," *IEEE Access*, vol. 4, pp. 7313–7321, Nov. 2016.
- [20] M. Cicerone, O. Simeone and U. Spagnolini, "Channel estimation for MIMO-OFDM systems by modal analysis/filtering," *IEEE Transactions on Communications*, vol. 54, no. 11, pp. 2062–2074, Nov. 2006.
- [21] E. Fishler and H. V. Poor, "Estimation of the number of sources in unbalanced arrays via information theoretic criteria," *IEEE Transactions on Signal Processing*, vol. 53, no. 9, pp. 3543–3553, Sept. 2005.
- [22] E. Fishler, M. Grosmann and H. Messer, "Detection of signals by information theoretic criteria: general asymptotic performance analysis," *IEEE Transactions on Signal Processing*, vol. 50, no. 5, pp. 1027–1036, May 2002.
- [23] K. Gomadam, V.R. Cadambe and S.A. Jafar, "Approaching the capacity of wireless networks through distributed interference alignment," in *Proc. of IEEE GLOBECOM*, pp. 1–6 New Orleans, LO, USA, Nov 30–Dec 4, 2008.
- [24] S.W. Peters and R.W. Heath, "Cooperative algorithms for MIMO interference channels," *IEEE Transactions on Vehicular Technology*, vol. 60, no. 1, pp. 206–218, Oct. 2011.
- [25] S.A. Jafar and M.J. Fakhereddin, "Degrees of freedom for the MIMO interference channel," *IEEE Transactions on Information Theory*, vol. 53, no. 7, pp. 2637–2642, June 2007.
- [26] M. Razaviyayn, G. Lyubeznik and Z.Q. Luo, "On the degrees of freedom achievable through interference alignment in a MIMO interference channel," *IEEE Transactions on Signal Processing*, vol. 60 no. 2, pp. 812–821, Feb. 2012.
- [27] S.R. Krishnamurthy, A. Ramakrishnan and S.A. Jafar, "Degrees of freedom of rank-deficient MIMO interference channels," *IEEE Transactions on Information Theory*, vol. 61, no. 1, pp. 341–365, Jan. 2015.
- [28] Y. Zeng, X. Xu, Y.L. Guan, E. Gunawan and C. Wang, "Degrees of freedom of the three-user rank-deficient MIMO interference channel," *IEEE Transactions on Wireless Communications*, vol. 13, no. 8, pp. 4179–4192, Aug. 2014.
- [29] L. Yang and W. Zhang, "On degrees of freedom region of three-user MIMO interference channels," *IEEE Transactions on Signal Processing*, vol. 63, no. 3, pp. 590–603, Feb. 2015.
- [30] H. Sun, S.R. Krishnamurthy and S.A. Jafar, "Rank matching for multihop multiflow," *IEEE Transactions on Information Theory*, vol. 61, no. 9, pp. 4751–4764, June 2015.
- [31] Ettus Research, "Software-defined radio device: USRP N210," available at www.ettus.com/product/details/UN210-KIT
- [32] Ettus Research, "OctoClock-G CDA-2990," available at www.ettus.com/product/details/OctoClock-G
- [33] E. Blossom, "GNU Radio: Tools for Exploring the Radio Frequency Spectrum," *Linux Journal*, vol. 2004, no. 122, 2004.
- [34] J.P. Kermoal, L. Schumacher, K.I. Pedersen, P.E. Mogensen and F. Frederiksen, "A stochastic MIMO radio channel model with experimental validation," *IEEE Journal on Selected Areas in Communications*, vol. 20, no. 6, pp. 1211–1226, Aug. 2002.
- [35] K. Yu, M. Bengtsson, B. Ottersten, D. McNamara, P. Karlsson, and M. Beach, "Modeling of wide-band MIMO radio channels based on NLoS indoor measurements", *IEEE Transactions on Vehicular Technology*, vol. 53, no. 3, pp. 655–665, May 2004.
- [36] R.K. Mallik, "The exponential correlation matrix: Eigen-analysis and applications," *IEEE Transactions on Wireless Communications*, vol. 17, no. 7, pp. 4690–4705, July 2018.
- [37] J. Choi and D.J. Love, "Bounds on eigenvalues of a spatial correlation matrix", *IEEE Communications Letters*, vol. 18 no. 8, pp. 1391–1394, Aug. 2014.
- [38] D. Gesbert, H. Bolcskei, D.A. Gore, and A.J. Paulraj, "Outdoor MIMO wireless channels: Models and performance prediction," *IEEE Transactions on Communications*, vol. 50, no. 12, pp. 1926–1934, Dec. 2002.
- [39] H. Shin and J.H. Lee, "Capacity of multiple-antenna fading channels: Spatial fading correlation, double scattering, and keyhole". *IEEE Transactions on Information Theory*, vol. 49, no. 10, pp. 2636–2647, Oct. 2003.
- [40] C. Eckart, and G. Young, "The approximation of one matrix by another of lower rank," *Psychometrika*, vol. 1, no. 3, pp. 211–218, 1936.
- [41] 3GPP TR 36.842, "Study on Small Cell enhancements for E-UTRA and E-UTRAN; Higher layer aspects." Available: <https://portal.3gpp.org/desktopmodules/Specifications/SpecificationDetails.aspx?specificationId=2543>
- [42] IEEE 802.11ac, "IEEE standard for information technology-telecommunications and information exchange between systems-Local and metropolitan area networks-specific requirements-Part 11: Wireless LAN medium access control (MAC) and physical layer (PHY) specifications-amendment 4: enhancements for very high throughput for operation in bands below 6 GHz," *IEEE Standards 802.11ac*, Dec. 2013.
- [43] X. Xie, X. Zhang, and K. Sundaresan, "Adaptive feedback compression for MIMO networks," in *Proc. of ACM MobiCom*, pp. 477–488, Miami, FL, Sep. 2013.
- [44] X. Zhang, K. Sundaresan, M.A. Khojastepour, S. Rangarajan, and K.G. Shin, "NEMOx: scalable network MIMO for wireless networks," in *Proc. of ACM MobiCom*, pp. 453–464, Miami, FL, Sep. 2013.
- [45] O. Bejarano, E. Magistretti and O. Gurewitz, "Mute: sounding inhibition for MU-MIMO WLANs," in *Proc. of IEEE SECON*, pp. 135–143, Singapore, June 30–July 3, 2014.
- [46] X. Xie and X. Zhang, "Scalable user selection for MU-MIMO networks," in *Proc. of IEEE INFOCOM*, pp. 808–816, Toronto, Canada, April 27–May 2, 2014.
- [47] C. Shepard, H. Yu, N. Anand, E. Li, T. Marzetta, R. Yang and L. Zhong, "Argos: practical many-antenna base stations," in *Proc. of ACM MobiCom*, pp. 53–64, Istanbul, Turkey, Aug. 2012.
- [48] G.S. Smith, "A direct derivation of a single-antenna reciprocity relation for the time domain," *IEEE Transactions on Antennas and Propagation*, vol. 52, no. 6, pp. 1568–1577, June 2004.
- [49] Y. Chen, Y. Huang, Y. Shi, Y.T. Hou, W. Lou and S. Kompella, "On DoF-based interference cancellation under general channel rank conditions," *IEEE/ACM Transactions on Networking*, vol. 28, no. 3, pp. 1002–1016, June 2020.
- [50] F.P. Kelly, A.K. Maulloo and D.K.H. Tan, "Rate control for communication networks: Shadow prices, proportional fairness and stability," *The Journal of the Operational Research Society*, vol. 49, no. 3, pp. 237–252, April 1998.
- [51] A. Ben-Tal and A. Nemirovski, *Lectures on modern convex optimization: analysis, algorithms, and engineering applications*, Chapter 3, SIAM, 2001. ISBN: 9780898714913.
- [52] Gurobi Optimization, Inc. "Gurobi optimizer reference manual," 2018. Available: <http://www.gurobi.com>
- [53] B. Hochwald and S. Vishwanath, "Space-time multiple access: Linear growth in the sum rate", in *Proc. 40th Annual Allerton Conf. Communications, Control and Computing*, Monticello, IL, USA, Oct. 2002.
- [54] Q. Wang and Y. Jing, "New rank detection methods for reduced-rank MIMO systems," *EURASIP Journal on Wireless Communications and Networking*, vol. 2015, no. 1, pp. 230, Oct. 2015.
- [55] M. Nicoli and U. Spagnolini, "Reduced-rank channel estimation for time-slotted mobile communication systems," *IEEE Transactions on Signal Processing*, vol. 53, no. 3, pp. 926–944, March 2005.
- [56] A.G. Burr, "Capacity bounds and estimates for the finite scatterers MIMO wireless channel," *IEEE Journal on Selected Areas in Communications*, vol. 21, no. 5, pp. 812–818, June 2003.
- [57] C.R. Johnson and J. A. Link, "Solution theory for complete bilinear systems of equations," *Numerical Linear Algebra with Applications*, vol. 16, no. 11–12, pp. 929–934, Nov./Dec. 2009.



Yongce Chen (M'21) is currently a Senior System Software Engineer at NVIDIA Corporation, Santa Clara, CA, USA. He received his Ph.D. degree in electrical engineering from Virginia Tech, Blacksburg, VA, USA, in 2021, and his B.S. and M.S. degrees in electrical engineering from Beijing University of Posts and Telecommunications (BUPT), Beijing, China, in 2013 and 2016, respectively. During his Ph.D. study at Virginia Tech, he was awarded a VT Wireless Fellowship in 2016 and a Pratt Fellowship in 2021, respectively.

He received the Best Paper Award in IEEE INFOCOM 2021. His current research interests include optimization, MIMO techniques and real-time implementation for wireless networks.



Y. Thomas Hou (F'14) is Bradley Distinguished Professor of Electrical and Computer Engineering at Virginia Tech, Blacksburg, VA, USA, which he joined in 2002. He received his Ph.D. degree from NYU Tandon School of Engineering (formerly Polytechnic Univ.) in 1998. During 1997 to 2002, he was a Member of Research Staff at Fujitsu Laboratories of America, Sunnyvale, CA, USA. Prof. Hou's current research focuses on developing innovative solutions to complex science and engineering problems arising from

wireless and mobile networks. He is also interested in wireless security. He has published over 300 papers in IEEE/ACM journals and conferences. His papers were recognized by nine best paper awards from IEEE and ACM. He holds six U.S. patents. He authored/co-authored two graduate textbooks: *Applied Optimization Methods for Wireless Networks* (Cambridge University Press, 2014) and *Cognitive Radio Communications and Networks: Principles and Practices* (Academic Press/Elsevier, 2009). Prof. Hou was named an IEEE Fellow for contributions to modeling and optimization of wireless networks. He was/is on the editorial boards of a number of IEEE and ACM transactions and journals. He served as Steering Committee Chair of IEEE INFOCOM conference and was a member of the IEEE Communications Society Board of Governors. He was also a Distinguished Lecturer of the IEEE Communications Society.



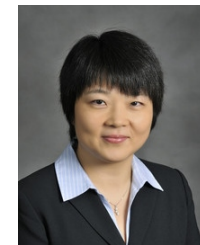
Shaoran Li (S'17) received his B.S. degree from Southeast University, Nanjing, China, in 2014 and M.S. degree from Beijing University of Posts and Telecommunications (BUPT), Beijing, China in 2017. Currently, he is a Ph.D. student at Virginia Tech supervised by Professor Thomas Hou. His research interests are algorithm design and implementation for wireless networks.



Chengzhang Li (S'17) is a Ph.D. student in the Bradley Department of Electrical and Computer Engineering at Virginia Tech, Blacksburg, VA, USA. He received his B.S. degree in Electronics Engineering from Tsinghua University, Beijing, China, in 2017. His current research interests are modeling, analysis and algorithm design for wireless networks, with a focus on Age of Information (AoI) and latency research.



Brian Jalaian (M'15) is a research scientist and technical research lead at Army Research Laboratory and a adjunct research assistant professor at Virginia Tech. He has obtained his Ph.D. from the Bradley Department of Electrical and Computer Engineering in 2016 at Virginia Tech. He has obtained his MS in Electrical Engineering (Network and Communication Systems) and MS in Industrial System Engineering (Operation Research) in 2013 and 2014 at Virginia Tech, respectively. His research interests are optimization, machine learning, and network science.



Wenjing Lou (F'15) is the W. C. English Endowed Professor of Computer Science at Virginia Tech and a Fellow of the IEEE. She holds a Ph.D. in Electrical and Computer Engineering from the University of Florida. Her research interests cover many topics in the cybersecurity field, with her current research interest focusing on wireless networks, privacy protection in machine learning systems, and security and privacy problems in the Internet of Things (IoT) systems. Prof. Lou is a highly cited researcher by the Web of Science Group. She received the Virginia Tech Alumni Award for Research Excellence in 2018, which is the highest university level faculty research award. She received the INFOCOM Test-of-Time paper award in 2020. She is the TPC chair for IEEE INFOCOM 2019 and ACM WiSec 2020. She was the Steering Committee Chair for IEEE CNS conference from 2013 to 2020. She is currently a steering committee member of IEEE INFOCOM and IEEE Transactions on Mobile Computing. She served as a program director at US National Science Foundation (NSF) from 2014 to 2017.



Huacheng Zeng (SM'20) is an Assistant Professor in the Department of Computer Science and Engineering at Michigan State University (MSU). Prior to joining MSU, he was an Assistant Professor of Electrical and Computer Engineering at University of Louisville and a Senior System Engineer at Marvell Semiconductor. He holds a Ph.D. degree in Computer Engineering from Virginia Polytechnic Institute and State University. He was a recipient of NSF CAREER Award. His research interest is broadly in computer networking and sensing systems.